HHS Public Access

Author manuscript

Mol Biol Cell. Author manuscript; available in PMC 2026 February 18.

Published in final edited form as:

Mol Biol Cell. 2025 December 01; 36(12): ar145. doi:10.1091/mbc.E24-12-0539.

Patient-derived induced pluripotent stem cells with a C9orf72 expansion as a model to study frontotemporal dementia pathologies

Sonia Infante-Tadeo, **Diane L. Barber***

Department of Cell and Tissue Biology, University of California San Francisco, San Francisco, CA 94941

Abstract

The neurodegenerative disorder frontotemporal dementia (FTD) can be caused by a repeat expansion (GGGGCC; G4C2) in C9orf72. The function of wild-type C9orf72 and the mechanism by which the C9orf72-G4C2 expansion causes FTD, however, remain unresolved. Diverse disease models, including human brain samples and differentiated neurons from patient-derived induced pluripotent stem cells (iPSCs), identified some hallmarks associated with FTD, but these models have limitations, including biopsies capturing only a static snapshot of dynamic processes and differentiated neurons being labor-intensive, costly, and postmitotic. We find that patient-derived iPSCs, without being differentiated into neurons, exhibit established FTD hallmarks, including increased lysosome pH, decreased lysosomal cathepsin activity, cytosolic TDP-43 proteinopathy, and increased nuclear TFEB. Moreover, lowering lysosome pH in FTD iPSCs mitigates TDP-43 proteinopathy, suggesting a key role for lysosome dysfunction. RNA-seq reveals dysregulated transcripts in FTD iPSCs affecting calcium signaling, cell death, synaptic function, and neuronal development. We confirm differences in protein expression for some dysregulated genes not previously linked to FTD, including ciliary neurotrophic factor receptor (neuronal survival), Annexin A2 (anti-apoptotic), NANOG (neuronal development), and Moesin (cytoskeletal dynamics). Our findings underscore the potential of FTD iPSCs as a model for studying FTD cellular pathology and for drug screening to identify therapeutics.

INTRODUCTION

Alterations in C9orf72 are the most common inherited genetic cause of frontotemporal dementia (FTD) as well as amyotrophic lateral sclerosis (ALS; Sonobe et al., 2023; Todd et al., 2023). FTD, a dementia related to Alzheimer's disease (AD), commonly affects individuals aged less than 65 years old. Genetic factors contribute to 30–40% of FTD cases, with alterations in C9orf72 being the most prevalent, but FTD is also associated with

*correspondence to: Diane L. Barber (diane.barber@ucsf.edu).

Author contributions: D.L.B. conceived the hypothesis. D.L.B. and S.I.-T. designed the study, developed experiments, and obtained and analyzed data as well as assembled figures and wrote the manuscript.

Conflicts of interest: The authors declare no competing financial interests.

mutations in progranulin (GRN) or tau (MAPT; Greaves and Rohrer, 2019). Alterations in C9orf72 associated with FTD are typically a hexanucleotide (GGGGCC [G4C2]) repeat expansion (DeJesus-Hernandez et al., 2011; Renton et al., 2011). While healthy individuals typically possess fewer than 20 G4C2 repeats, expansions from 30 to more than 100 repeats are linked to ALS and FTD (Rademakers et al., 2012; Babic Leko et al., 2019). Common cellular abnormalities associated with C9orf72-G4C2 include a disrupted endolysosomal pathway, increased lysosomal pH (pHlys), reduced lysosomal hydrolase activity, and TDP-43 proteinopathy, which collectively contribute to cell damage (Ling et al., 2013; Amick and Ferguson, 2017). Although the role of wild-type C9orf72 in maintaining lysosome balance is acknowledged (Amick and Ferguson, 2017), the mechanisms whereby mutant C9orf72-G4C2 leads to impaired lysosome biology, toxicity, and neurodegeneration remain unclear (Babic Leko et al., 2019).

Our current understanding of FTD pathogenesis comes from different experimental models, each with advantages and limitations. Postmortem brain samples from FTD patients provide in situ analysis and tissue-level pathologies but capture only a static snapshot of dynamic processes and are not amenable to genetic manipulation for mechanistic analysis or drug screening to identify potential therapeutics (Halliday et al., 2011; Irwin et al., 2015). Models in mice (Chew et al., 2015; Czuppa et al., 2022; Lopez-Herdoiza et al., 2023) and models with other organisms, including zebrafish (Shaw et al., 2018) and Drosophila (Mizielinska et al., 2014), provide systems-level and genetic manipulation but with species differences that do not effectively recapitulate human FTD (Neumann and Mackenzie, 2019; Ahmed et al., 2023; White et al., 2024). An increasingly used cellular model is neurons differentiated from induced pluripotent stem cells (iPSCs) generated from patients with FTD (Lee and Huang, 2017; Beckers and Van Damme, 2024). Using differentiated neurons reveals several key findings, including changes in lysosomal cathepsin activity (Lee and Huang, 2017; Valdez et al., 2017), aberrant cytosolic aggregates of TDP-43, and dysregulated TFEB and TFE3, which are transcription factors regulating lysosome biogenesis. However, despite recently improved protocols to differentiate neurons from iPSCs (Espuny-Camacho et al., 2013; Raitano et al., 2015; Qi et al., 2017), the procedure remains time-extensive and costly, and the most streamlined methods require genetic manipulations (Lara Flores et al., 2023). Moreover, as postmitotic cells, terminally differentiated neurons cannot be propagated for continual use. To our knowledge, the use of FTD patient-derived iPSCs as a tractable experimental model without differentiation to neurons has received limited attention, indicating a potential avenue for further investigation (Selvaraj et al., 2017; Lines et al., 2020). In contrast, ALS patient-derived iPSCs have been used as a model system for examining epigenetic perturbations caused by C9orf72 expansions (Esanov et al., 2016).

In this report, we tested the feasibility of using iPSCs as a tractable model for studying FTD cellular pathologies. We compared iPSCs derived from patients with FTD carrying a C9orf72-G4C2 expansion (FTD1: male, 48 years old; FTD2: female, 65 years old) with control wild-type iPSCs (WT: male, 64 years old) from a nonaffected individual. The WT line was gender-matched to FTD1 and age-matched to FTD2, and race-matched to both FTD lines. Defective lysosomal acidification causes neuroinflammation and neurodegeneration through a variety of detrimental cellular pathways (Quick et al., 2023). We found that FTD iPSCs have hallmarks of FTD-associated pathologies, including increased pHlys,

decreased cathepsin activity, TDP-43 proteinopathy with cytoplasmic aggregates, and nuclear accumulation of TFEB, which are consistent with findings in patient tissues (Smeele et al., 2024) and neurons differentiated from iPSCs (Lee and Huang, 2017; Valdez et al., 2017). Furthermore, RNA-seq analysis identified transcriptomic differences in FTD1 iPSCs compared with WT iPSCs, including dysregulated genes involved in neuroinflammation, calcium signaling, synaptic function, and neuronal development not previously linked to FTD. The significance of our findings includes 1) confirming that dysregulated cell functions with C9orf72-G4C2 are not limited to neurons, 2) identifying new regulators of dysregulated cell functions with FTD, and 3) showing the promise of using FTD iPSCs as a previously unreported experimental model for investigating FTD cellular pathologies and as a platform for drug screening to identify therapeutics for treating FTD (Vo et al., 2024).

RESULTS

Our study used iPSCs sourced from the National Institute of Neurological Disorders and Stroke (NINDS), including cells derived from an FTD-affected 48-year-old Caucasian male with a C9orf72-G4C2 expansion (FTD1 iPSCs) and a nonaffected gender and race-matched individual (wild-type [WT] iPSCs). We confirmed the pluripotent state of both cell lines with standard markers and found no differences between WT compared with FTD1 iPSCs for the characteristics we determined, including colony morphology (Supplemental Figure S1A), E-cadherin abundance and localization at cell-cell junctions (Supplemental Figure S1 B, E), and predominantly nuclear localization of stem cell pluripotency transcription factors OCT4 and SOX2 (Supplemental Figure S1, C and D) as well as total abundance of OCT4 (Supplemental Figure S1 E).

FTD iPSCs have increased lysosome pH

Although the exact mechanisms triggering FTD pathologies with C9orf72-G4C2 remain unclear, an aberrantly high pHlys is reported with early stages of different types of neurodegeneration (Wolfe et al., 2013; Nixon, 2020; Chin et al., 2022). We therefore quantified pHlys by generating WT and FTD1 iPSCs stably expressing a genetically encoded and ratiometric fluorescent biosensor, pHLARE, which we previously described accurately measures pHlys within the range of pH 4.0 to 6.5 (Webb et al., 2021). pHLARE encodes the Lysosomal Associated Membrane Protein 1 (LAMP1) tagged at the lumenal domain with superfolder GFP and at the cytosolic domain with mCherry. We stably expressed in iPSC lines pHLARE containing an EF-1α promoter inserted into the AAVS1 harbor locus, which is a site commonly used for stable expression in stem cells (Smith et al., 2008), by using MaxCyte ATX electroporation and FACS sorting for mCherry. Measuring changes in ratiometric pHLARE calibrated to pH values with nigericin buffers at the end of each determination, as described (Webb et al., 2021), we found that the pHlys of FTD1 iPSCs, 5.0 ± 0.2, was significantly higher compared with WT iPSCs, 4.4 ± 0.2 (Figure 1, A and B). To validate our findings obtained with pHLARE, we performed ratiometric fluorescence imaging using the pH-sensitive dye Oregon Green 488 Dextran. Consistent with the pHLARE measurements, WT iPSCs showed an average pH of 5.4 ± 0.8, whereas FTD1 iPSCs showed an increased average pH of around 6.1 ± 0.8 (Supplemental Figure S2A). Using Oregon Green 488 Dextran, we observed a comparable increase in pHlys in a

second FTD iPSC line (FTD2), derived from a 65-year-old Caucasian female FTD patient, and hence age- and ethnicity-matched with WT iPSCs (Supplemental Figure S2B). We also confirmed a predominant nuclear localization of the pluripotency marker OCT4 in FTD2 iPSCs (Supplemental Figure S2C). The slightly higher pH detected with Oregon Green 488 Dextran compared with pHLARE likely reflects lower specificity for lysosomes, as the dye is also distributed in late endosomes (Halcrow et al., 2021). Compared with previous findings, a higher pHlys is also seen in ALS iPSC-derived neurons (Lo and Zeng, 2023), in fibroblasts from Parkinson's disease (PD) patients (Colacurcio and Nixon, 2016), and in iPSC-derived neurons (i-neurons) from a patient carrying a common FTD-linked mutation in the GRN locus (Elia et al., 2023).

Despite the higher pHlys we observed in FTD iPSCs, immunoblotting total cell lysates revealed that WT and FTD1 iPSCs had a similar abundance of proteins reported to regulate pHlys, including LAMP1 and Transmembrane protein 175 (TMEM175; Figure 1C). TMEM175 was recently identified as a lysosomal K^+-H^+ channel with a pivotal role in maintaining lysosomal membrane potential and pHlys stability (Hu et al., 2022; Tang et al., 2023). LAMP1 was subsequently shown to bind to TMEM175 and regulate channel activity and pHlys (Zhang et al., 2023). Additionally, despite defective endolysosomal trafficking reported as an FTD pathology (Farg et al., 2014; Shi et al., 2018; Shao et al., 2022), WT and FTD1 iPSCs had a similar abundance of Ras-related protein Rab7 (Figure 1C), which confers maturation of late endosomes into lysosomes and lysosomal trafficking. These data are consistent with previous findings indicating no significant differences in LAMP1 expression within the frontal grey matter of FTD-C9orf72 individuals compared with control samples (Marian et al., 2023) or progranulin-deficient FTD cells (Valdez et al., 2017), as well as no significant difference in Rab7 expression in C9orf72 knockout mice (Todd et al., 2023).

Using several different approaches, we confirmed experimentally changing pHlys in both WT and FTD1 iPSCs. The pHlys of WT iPSCs increased with Bafilomycin A1 (Baf A1; 100 nM), an inhibitor of the vacuolar V-ATPase, the main proton pump in lysosomes (Tu et al., 2008; Casey et al., 2010), and chloroquine (CQ; 100 μM), an alkalinizing lysosomotropic compound (Levine and Kroemer, 2008; Tu et al., 2008), but did not change with Torin-1 (100 nM), an ATP-competitive inhibitor of mammalian target of rapamycin complex 1 (mTORC1) activity that lowers pHlys in somatic cells (Thoreen et al., 2009; Webb et al., 2021; Figure 1D). In contrast, in FTD1 iPSCs Torin-1 lowered pHlys, but Bafilomycin A1 had no effect (Figure 1E). We also found that the pHlys of both WT and FTD1 iPSCs were decreased when cells were treated with 4-(2-(6,7-Dichloro-2-cyclopentylindan-1-on-5-yl)ethyl)benzene-1,3-diol (DCPIB; 10 μM), which is reported to be a selective inhibitor of volume-regulated anion channels (VRACs) or swelling-activated chloride channels (Decher et al., 2001; Sardini et al., 2003; Figure 1, D and E). In contrast to DCPIB inhibiting VRACs and chloride channels, Hu and colleagues (Hu et al., 2022) reported that DCPIB targets TMEM175 to increase channel activity and pHlys in HEK293T cells.

Although FTD1 iPSCs had a higher pHlys compared with WT, their cytosolic pH (pHi) was not different (WT 7.57 ± 0.04, FTD1 7.55 ± 0.04; Supplemental Figure S2D), determined in cell populations loaded with the fluorescence pH-sensitive dye 2 ,7 - Bis(2-

carboxyethyl)-5(6)-carboxyfluorescein (BCECF). Additionally, DCPIB did not affect pHi of either WT or FTD1 iPSCs (Supplemental Figure S2D), suggesting a selective effect on pHlys. These findings are in contrast with studies, albeit limited, indicating that decreased pHi is associated with AD and other neurodegenerative diseases (Fang et al., 2010; Majdi et al., 2016), although to our knowledge, differences in pHi with FTD1 have not been reported.

Lysosome size is noted to be variable but generally ranges between 150–2000 nm, as determined in epithelial cells (Bandyopadhyay et al., 2014; Webb et al., 2021; Siddiqui and Bhatt, 2023). We found that WT and FTD1 had a mostly similar profile of lysosome size, including a mean size of 400 ± 235 nm for WT iPSCs and 500 ± 410 nm for FTD1 iPSCs. However, WT iPSCs had a greater number of smaller lysosomes between 200–300 nm, whereas FTD1 iPSCs had a higher proportion of larger lysosomes >1400 nm (Figure 1F). A similar finding of increased proportion of enlarged lysosomes is reported using transmission electron microscopy of C9orf72 iPSC-derived motor neurons (Beckers et al., 2023). Together, our findings indicate that compared with WT iPSCs, FTD iPSCs had a higher pHlys and somewhat larger lysosome size but no difference in pHi or the expression of LAMP1, TMEM175, and Rab7.

Proteolytic activity and Cathepsin B activity and expression are decreased in FTD iPSCs

Degradation of macromolecules and proteins in lysosomes relies on over 50 hydrolases, including many cathepsins with optimal activity in an acidic environment (Wolfe et al., 2013). We evaluated lysosomal hydrolase activity by staining cells with DQ-Red BSA, a fluorogenic substrate that is internalized through endocytosis and transported to endosomes and lysosomes. In acidic compartments, the BSA is degraded by lysosomal hydrolases, releasing BODIPY dye molecules. To confirm this behavior of DQ-Red BSA, we showed significantly decreased fluorescence in WT iPSCs treated with Bafilomycin A1 (100 nM, 18 h) (Figure 2A), which increased pHlys (Figure 1D). In control FTD1 cells, we found decreased fluorescence compared with control WT iPSCs (Figure 2A), indicating a lower proteolytic degradation. However, fluorescence increased to that seen in control WT iPSCs when we treated FTD1 iPSCs with Torin or DCPIB (Figure 2A), which lowered pHlys (Figure 1E).

Consistent with the higher pHlys in FTD1 compared with WT iPSCs and the reduced hydrolase activity observed in FTD1 iPSCs, the latter also had decreased cathepsin B activity (Figure 2, B and C), determined by staining with Magic Red, a fluorogenic reporter specifically cleaved by cathepsin B in lysosomes. FTD1 iPSCs, in addition to having decreased cathepsin B activity, also had decreased cathepsin B abundance compared with WT, determined by immunoblotting total cell lysates (Figure 2, D and E). Although decreased activity of lysosomal cathepsin D is seen in iPSC-derived cortical neurons from FTD1 patients harboring progranulin mutations (Valdez et al., 2017), to our knowledge, a link between C9orf72-G4C2 and decreased cathepsin B activity has not been reported. However, decreased cathepsin B abundance is seen in the cerebrospinal fluid of patients with primary progressive aphasia, a language variant of FTD (Swift et al., 2024). Additionally, inhibiting cathepsin B activity or its loss is reported to promote the development of AD and neurodegeneration (Kos et al., 2022). Additionally, previous studies highlighted that bone

marrow-derived cells exposed to pHlys-elevating chemicals have a notable reduction in both cathepsin B and D protein abundance (Xu et al., 2024). Together, our data confirm that a higher pHlys correlates with decreased total hydrolase activity, determined with DQ-Red BSA, and specifically cathepsin B activity, determined with Magic Red.

Cytosolic protein aggregates, including TDP-43, are increased in FTD iPSCs

Aberrant cytosolic protein aggregation is a hallmark of neurodegenerative diseases such as AD, PD, ALS, and FTD (Taylor et al., 2002; Neumann et al., 2006). We scored for global protein aggregates by using the PROTEOSTAT Aggresome Detection Reagent, a molecular rotor dye designed to interact with and disrupt the cross-beta spine of quaternary protein structures commonly found in misfolded and aggregated proteins. In WT iPSCs, the cytoplasmic fluorescence intensity was relatively low with a mean of 250 arbitrary units (a.u.), but increased with Bafilomycin A1 treatment (100 nM, 2 h) to a mean of 400 a.u. (Figure 3, A and B). In FTD1 iPSCs, the mean of 500 a.u. was greater than WT iPSCs, both control and treated with Bafilomycin A1 (Figure 3, A and B).

To further analyze the proteinopathy in FTD1 iPSCs, we immunolabeled for TAR DNA-binding protein 43 (TDP-43), a multi-functional DNA/RNA-binding protein found in both the nucleus and cytoplasm (Babic Leko et al., 2019; Lines et al., 2020; Ratti et al., 2020). Decreased nuclear TDP-43 and increased cytosolic TDP-43 aggregates are a common FTD pathology seen in a mouse model with a C9orf72 expansion (Shao et al., 2022), in affected neurons of patients with FTD (Neumann et al., 2006; Beckers and Van Damme, 2024), in postmortem brain tissue from FTD patients with C9orf72 expansions (Marian et al., 2023), and in neurons differentiated from iPSCs generated from a patient with FTD having decreased PGRN expression (Valdez et al., 2017). Consistent with these findings, immunolabeling showed that FTD1 iPSCs had a lower nuclear to cytoplasmic ratio of TDP-43 and visibly more cytosolic TDP-43 aggregates (Figure 4, A–C) compared with WT iPSCs; however, immunoblotting indicated that the abundance of total TDP-43 was not different in the two cell lines (Figure 4D). Similar results were observed for FTD2 iPSCs, which also had a lower nuclear to cytoplasmic ratio of TDP-43 and increased cytosolic aggregates compared with WT (Supplemental Figure S3, A and B). FTD1 iPSCs also had increased phosphorylated TDP-43 (pTDP-43) compared with WT, determined by immunoblotting cell lysates using pTDP-43 (Ser409/410; Figure 4E), which are residues commonly phosphorylated in pathological TDP-43 aggregates in ALS/FTD models (Rojas-Prats et al., 2021; Hung et al., 2023). Disrupted endolysosomal trafficking is suggested to be a major determinant in TDP-43 proteinopathy (Shao et al., 2022); however, a role for increased pHlys is also indicated in TDP-43 proteinopathy as seen in HeLa cells treated with Bafilomycin A1 (Tanaka et al., 2023). Consistent with Bafilomycin A1 increasing pHlys in WT iPSCs, it also decreased the nuclear to cytoplasmic ratio of TDP-43 and enhanced cytosolic TDP-43 aggregates (Figure 4F). Also, consistent with DCPIB decreasing pHlys in FTD1 iPSCs, it increased the nuclear to cytoplasmic ratio of TDP-43 and attenuated cytosolic TDP-43 aggregates compared with untreated control FTD1 cells (Figure 4G). The TDP-43 nuclear to cytoplasmic ratio in FTD1 iPSCs treated with DCPIB was only partially rescued (mean 14.24 ± 0.65 SEM) compared with control WT iPSCs (mean 22.06 ± 0.84), perhaps because of the short (24 h) treatment time. These findings underscore

the association between increased pHlys and increased TDP-43 proteinopathy, suggesting targeting pHlys or using DCPIB as a potential therapeutic to reduce TDP-43 proteinopathy in FTD.

FTD iPSCs have increased nuclear TFEB but similar total TFEB protein abundance compared with WT iPSCs

TFEB, a member of the MiTF/TFE transcription factor family, regulates the transcription of coordinated lysosomal expression and regulation (CLEAR) genes involved in autophagy and lysosome biogenesis, including lysosomal membrane proteins and hydrolases (Cho and Hwang, 2012; Wang et al., 2018; Ojalvo-Pacheco et al., 2024). Under normal conditions, phosphorylated TFEB remains in the cytosol, but during starvation or lysosomal stress, it is dephosphorylated and translocated to the nucleus, activating lysosomal biogenesis (Cho and Hwang, 2012; Shariq et al., 2024). Immunolabeling for TFEB showed a greater nuclear to cytoplasmic ratio in FTD1 compared with WT iPSCs (Figure 5, A–C), which is consistent with our findings that FTD1 iPSCs had more large lysosomes compared with WT (Figure 1F) and lysosomal enlargement activating TFEB (Wang et al., 2018). Cytosolic TFEB in FTD1 iPSCs, however, was not notably in aggregates (Figure 5B) like we observed with TDP-43 (Figure 4B). Immunoblotting showed that FTD1 iPSCs had less phosphorylated TFEB than WT, but the total TFEB levels were similar (Figure 5D), consistent with phosphorylated TFEB being retained in the cytoplasm. Our findings are in agreement with previous reports indicating that loss of C9orf72 function in HEK293T cells leads to nuclear translocation of TFEB (Ugolino et al., 2016; Wang et al., 2020). In contrast to our findings, however, decreased nuclear TFEB expression was reported in postmortem brain samples of AD and ALS patients (Wang et al., 2016).

Lysosome biogenesis is also promoted by the activity of TFE3, a bHLH-leucine zipper transcription factor that, like TFEB, translocates from the cytoplasm to the nucleus when active and regulates autophagy (Jain et al., 2022; Mutvei et al., 2023; Ojalvo-Pacheco et al., 2024). However, unlike the increased nuclear TFEB we observed in FTD1 compared with WT iPSCs, we observed no difference in TFE3 localization between the two cell lines (Supplemental Figure S4, A and B), determined by immunolabeling, or TFE3 abundance, determined by immunoblotting total cell lysates (Supplemental Figure S4C). The role of TFE3 in FTD is controversial. TFEB and TFE3 interact with different regulatory proteins and enzymes; therefore, changes in TFEB-specific regulators, such as mTORC1 or calcineurin, may selectively impact TFEB activity without influencing TFE3. Additionally, mutations in genes involved in TFEB regulation, such as CLEAR network genes, may disrupt TFEB function without directly affecting TFE3. Despite both TFEB and TFE3 having a conserved transcriptional activation domain, TFEB aggregation is facilitated by the PrLD domain, which is absent in TFE3, and suggested as a target in Huntington's disease (HD) (Ojalvo-Pacheco et al., 2024). Although C9orf72 expansion is associated with increased nuclear TFE3 (Wang et al., 2020), a general view is that dysregulated TFE3 localization may not be a hallmark of neurodegeneration (Ojalvo-Pacheco et al., 2024). Additionally, we saw no difference between FTD1 and WT iPSCs in the abundance of total or phosphorylated ULK1, a protein activated with autophagy stimulation (Amick and Ferguson, 2017; Root et al., 2021) (Supplemental Figure S4D). Our data indicate that

in FTD iPSCs, TFEB regulation was distinct from changes in TFE3, ULK, and pULK, highlighting the complexity of signaling networks whereby C9orf72-G4C2 affects lysosome biology.

Transcriptomic profiling reveals dysregulated pathways in FTD compared with WT iPSCs.

For unbiased insights on possible differences in gene expression and signaling networks in FTD compared with WT iPSCs, we used RNA sequencing (RNA-seq). A Venn diagram revealed the number of shared and unique transcript levels between WT and FTD1 (Figure 6A), with WT iPSCs having a total of 1476 differentially expressed genes (DEGs) with an adjusted q-value of less than 0.05 after batch correction. Of these DEGs, 433 were unique to WT compared with FTD1 iPSCs. FTD1 iPSCs had 1,904 DEGs, with 861 unique DEGs. WT and FTD1 shared 1043 DEGs, which is almost 45% of their total number of DEGs (Figure 6A). A volcano plot, with each dot representing a gene, revealed increased and decreased transcripts in FTD1 compared with WT iPSCs (Figure 6B), which could potentially be used as biomarkers. DEGs (q-value 0.05) are shown in blue, and we highlighted upregulated genes of interest in green and downregulated genes of interest in magenta based on literature mining (Figure 6B). Compared with WT iPSCs, FTD1 iPSCs had increased expression of genes associated with synaptic and cytoskeletal processes, including moesin (MSN) (Beckmann et al., 2023) and presynaptic scaffolding RIM family members (RIMS1, RIMS2, RIMS3, and RIMS4). Additionally, FTD1 IPSCs had increased expression of transcripts for synaptic regulation, such as CHGA and NNAT (Seredenina et al., 2011; Sathe et al., 2021; Podvin et al., 2022; Zou et al., 2022), as well as for inflammatory response, including MFGE8 (Almansoub et al., 2019) and IDO1 (Duan et al., 2020), which are linked to dementia. Similarly, FTD1 iPSCs had increased expression of several transcripts not previously associated with neurodegeneration, such as lysosome-associated H^+-coupled amino acid transporters, SLC36A1 and SLC36A4 (Thwaites and Anderson, 2011; Hu et al., 2022), the lysosomal stress response protein LGALS3BP (Pan et al., 2014), and the neurotransmitter release transcripts belonging to the SYT family (SYT4, SYT10, and SYT13; Südhof, 2012).

Gene transcripts decreased in FTD1 compared with WT iPSCs, including some previously lin ked to ALS, FTD, and/or PD, such as CHCHD2 (Imai et al., 2019), the ciliary neurotrophic factor receptor (CNTFR; Deolankar et al., 2021), the neuronal development regulator SATB2 (Espuny-Camacho et al., 2013), four zinc-finger transcription factors (ZNF208, ZNF728, ZNF492, and ZNF835), as well as AKT1, which is related to lysosomal function and dysregulation (Paquette et al., 2021). Based on RNA-sequencing (RNAseq) findings, we confirmed by immunoblotting decreased expression in FTD1 compared with WT iPSCs of Annexin A2, a Ca^{2+} binding antiapoptotic protein that regulates lysosome functions (Rentero et al., 2018; Quick et al., 2023) and CNTFR, which enhances neuronal survival (Yong et al., 2022) and has been associated with TDP-43 aggregation (Liao et al., 2022; Figure 6C). Recent insights from Grieve *et al.* (2025) identify Annexin A2 as a key regulator of endolysosomal trafficking, and its downregulation in FTD iPSCs may contribute to the trafficking and degradative defects we observed, including impaired lysosomal acidification and cathepsin activity. CNTFR is also downregulated in AD (Deolankar et al., 2021), although to our knowledge it has not been linked to FTD. In FTD1 iPSCs, we also

confirmed, by immunoblotting, decreased expression of the pluripotency factor NANOG (Figure 6C), which protects against neuronal toxicity (Chang et al., 2020). Immunoblotting confirmed that compared with WT iPSCs, FTD1 iPSCs have increased expression of the cytoskeletal linker MSN (Figure 6C), which was recently shown to mediate tau-induced neurodegeneration (Beckmann et al., 2023). Moesin upregulation has also been reported in HIV-associated dementia in macaques, which mirrors the human disease (Gersten et al., 2009).

Moreover, we used gene ontology (GO) enrichment analysis of DEGs with the Enrichr database to reveal differences between FTD1 and WT iPSCs in cellular components (increases for neuron projections and glutamate receptor complex), biological processes (increases for neurotransmitter and synaptic transmission; decreases in neuron differentiation), and molecular functions (increases Ca^{2+} and neurotransmitter activity; decreases in DNA binding components; Figure 6D). Dysregulated Ca^{2+} homeostasis is associated with neurodegenerative conditions leading to neuronal loss (Hadi et al., 2024). In summary, these data revealed widespread transcriptomic differences in FTD1 compared with iPSCs, highlighting potential biomarkers as well as possible therapeutic targets.

Consistent with its effect on pHlys, DCPIB treatment (10 μM, 24 h) of FTD1 iPSCs decreased expression of Moesin (MSN), which is elevated in untreated FTD1 iPSCs, and increased expression of Annexin A2 (ANXA2), which is reduced in untreated FTD1 iPSCs, thereby restoring levels toward those seen in WT iPSCs (Figure 6E). These findings suggest that DCPIB may act by stabilizing protein expression rather than through changes in gene transcription.

DISCUSSION

Motivated by the challenges and limitations of current FTD models, in this study, we explored cellular pathologies using patient-derived iPSCs having a mutant C9ofr72-G4C2 expansion as an experimental model. We found that FTD iPSCs had disease hallmarks previously reported in neuronal models, including a disrupted lysosome biology of increased pHlys and decreased lysosomal hydrolase activity, and specifically decreased cathepsin B activity, cytosolic protein aggregation, including TDP-43 proteinopathy, and increased nuclear TFEB. Furthermore, we found that pharmacologically decreasing pHlys attenuates TDP-43 proteinopathy in FTD iPSCs, highlighting the crucial role of lysosomal dysfunction in FTD. Moreover, RNAseq of FTD1 compared with WT iPSCs revealed dysregulated gene transcripts involved in calcium signaling, cell death, synaptic function, and neuronal development. Collectively, these findings underscore the potential of FTD iPSCs as a model for studying FTD cellular pathologies and for insights into signaling mechanisms regulated by C9orf72-G4C2.

We confirmed that pHlys was higher in FTD compared with WT iPSC by using two approaches: a genetically encoded pHlys biosensor, pHLARE, which we developed (Webb et al., 2021), and the dye Oregon Green that was previously used to measure pHlys (Canton and Grinstein, 2017). A higher pHlys is also reported in FTD caused by progranulin haploinsufficiency (Tanaka et al., 2017; Elia et al., 2023), AD caused by presenilin 1

deficiency (Lee et al., 2010), and altered activity of the PD-risk protein TMEM175 (Hu et al., 2022). Collectively, these findings suggest that increased pHlys may be a hallmark of neurodegenerative disorders, as previously proposed (Nixon, 2017; Root et al., 2021). Further studies are needed to determine how C9orf72-G4C2 causes increased pHlys, with FTD iPSCs being a feasible model for resolving mechanisms. Although FTD1 and WT iPSCs had no difference in expression of TMEM175, which has been reported to regulate pHlys (Zhang et al., 2023), we cannot rule out possible differences in TMEM175 activity. We did find that DCPIB, a previously reported inhibitor of VRAC and swelling-activated chloride channels (Decher et al., 2001; Sardini et al., 2003), decreased pHlys with no effect on pHi. Treating FTD1 iPSCs with DCPIB increased the reduced hydrolase activity and attenuated TDP-43 proteinopathy, and partially rescued disease-associated changes in Annexin A2 and Moesin protein levels, both of which were dysregulated in FTD1 compared with WT cells. Although not previously reported, of interest is whether DCPIB targets the lysosomal Cl-H exchanger ClC-7, which regulates pHlys (Graves et al., 2008; Coppola et al., 2023), and whether it might be considered as a therapeutic in treating FTD. Other possible regulators of increased pHlys in FTD cells are members of the SLC36 family of lysosomal proton-coupled amino acid transporters, as suggested by our RNA-seq data indicating increased expression of SLC36A1 and SLC36A4. Alternatively, although receiving limited attention relative to neurodegenerative diseases, it is unclear whether a higher pHlys changes the expression or activity of SLC36 family members and hence contributes to nutrient imbalances and dysregulated mTORC1 activity. Our finding that FTD1 iPSCs had a greater nuclear/cytoplasmic ratio of TFEB and less phosphorylated TFEB compared with WT iPSCs suggests decreased mTORC1 activity, although this remains to be confirmed.

Cytosolic accumulation and aggregates of TDP-43 are hallmarks of not only FTD (Greaves and Rohrer, 2019; Shao et al., 2022) but also other neurodegenerative disorders (Beckers and Van Damme, 2024), and lysosomal dysfunction may play a significant role in protein aggregate accumulation (Shao et al., 2022; Ojalvo-Pacheco et al., 2024). Of significance, our study showed that FTD1 and FTD2 iPSCs have cytoplasmic mislocalization of TDP-43 even in the absence of neuronal differentiation. Furthermore, immunoblotting revealed increased pTDP-43 in FTD1 iPSCs, a key marker of pathological aggregation. Reducing TDP-43 proteinopathy is a target for FTD therapeutics (Liao et al., 2022), and our results indicate that FTD iPSCs could be a tractable model toward achieving this goal and highlight the promise of targeting increased pHlys, which, when reduced by DCPIB, attenuated TDP-43 proteinopathy in FTD iPSCs.

Our RNAseq analysis highlights additional differences in FTD1 compared with WT iPSCs, particularly gene transcripts associated with synaptic regulation, including SYT family members, and neuronal development, including NANOG, SATB2, and ZNF transcription factors. RNA-seq data confirmed dysregulated expression of several genes previously associated with FTD, ALS, or PD, including decreased expression of CNTFR, CHCHD2, AKT1, and NANOG (Imai et al., 2019; Chang et al., 2020; de Araujo et al., 2020; Deolankar et al., 2021; Paquette et al., 2021). Also previously linked to neurodegenerative disorders is increased expression of MSN (Beckmann et al., 2023). For RNAseq data, we confirmed dysregulated expression of CNTFR, ANXA2, NANOG, and MSN by immunoblotting.

The role of Annexin A2 in endolysosomal membrane dynamics and fusion provides a plausible mechanistic link between its downregulation and the impaired lysosomal clearance observed in FTD1 iPSCs. Moreover, since Annexin A2 functions across cell types to regulate vesicular trafficking (Grewal et al., 2025), its dysregulation in undifferentiated iPSCs supports their relevance as a model to study early pathogenic events in FTD. Notably, in agreement with our immunoblotting data, RNAseq did not show differences in the expression of TMEM175, LAMP1, ULK, or Rab7.

Collectively, our findings support using iPSCs as a model for insights into the cell biology of FTD. Although C9orf72 binds to lysosomes (Amick and Ferguson, 2017), how wild-type and

C9orf72-G4C2 regulate lysosome functions remains controversial (Root et al., 2021). The FTD iPSCs we used with variations to correct C9orf72 expansions are an experimentally feasible model for resolving signaling networks and molecular mechanisms. Beyond C9orf72-G4C2 and FTD, iPSCs derived from patients having FTD and other neurodegeneration-causing mutations in MAPT/tau, progranulin, LRRK2, and PARK2 are available through the NINDS human cell repository (https://nindsgenetics.org/) and likely also useful for mechanistic insights on associated cell dysfunctions. Additionally, because of the time and cost-effective advantages of iPSCs compared with terminally differentiated neurons, we also suggest that iPSCs from affected patients are a feasible platform for drug screening to identify small molecules, for example, that lower pHlys, with promise as therapeutics for treating FTD and other neurodegenerative disorders. Neurons derived from iPSCs carrying the C9orf72-G4C2 expansion have been used for screening small libraries (2K bioactive compounds; Czuppa et al., 2022). However, iPSCs offer greater feasibility for screening larger libraries, especially when combined with genetically encoded biosensors such as pHLARE, which enables longitudinal screening to identify small molecules that lower pHlys.

MATERIALS AND METHODS

Request a protocol through *Bio-protocol*

Cell culture and transfection: Cell lines were obtained from the NINDS, including WT (NHCDR ID ND41866, Cell line ID NN0003921), FTD1 (NHCDR ID ND50037, Cell line ID NN0000035), and FTD2 (NHCDR ID ND50035, Cell line ID NN0000039) iPSCs. FTD1 iPSCs were generated from a disease-affected 48-year-old Caucasian male with a C9orf72-G4C2 expansion, and FTD2 iPSCs were generated from a 65-year-old Caucasian female also with a C9orf72-G4C2 expansion. WT iPSCs were generated from a nonaffected 64-year-old Caucasian male, gender-matched with FTD1 and age-matched with FTD2.

Cells were maintained in mTeSR Plus medium (STEMCELL Technologies) on Matrigel-coated dishes (Corning Matrigel hESC-Qualified Matrix) at 37°C and 5% CO_2 and passaged by using Accutase to dissociate cells. After dissociation, cell suspensions were centrifuged at 1000 rpm for 5 min, and the cell pellet was resuspended in mTeSR Plus medium supplemented with 10 μM of the Rho kinase inhibitor Y-27632 (MedChemExpress HY-10583) and plated on Matrigel-coated dishes. After 24 h, the medium was replaced with

mTeSR Plus lacking Y-27632. Mycoplasma contamination was tested twice a year using medium obtained from cells maintained for 48 h by using a PCR Mycoplasma Detection Kit (abm #G238). Cell lines were authenticated commercially by IDEXX Bio-Analytics.

Stable expression of pHLARE: A mammalian expression plasmid with a CMV promoter encoding pHLARE was generated by our laboratory as previously reported (Webb et al., 2021) and is commercially available (Addgene #164477). For stable expression in iPSCs, Gibson assembly was used to replace the CMV promoter with an EF-1α promoter. Confluent iPSCs, maintained as described above, were dissociated with Accutase, pelleted by centrifugation, and resuspended to 3–5 × 10^7 cells/ml in MaxCyte EP buffer containing Y27632 (10 μM), transferring 50 μl of cell suspension into a separate microcentrifuge tube for each transfection to which 240 μg/ml DNA/tube was added. For TALEN-mediated insertion to the AAVS1 locus, we used a 4:3:3 ratio, donor construct: each of the site-specific TALENs (TALEN L [Addgene #59025] and TALEN R [Addgene #59026]). The cell suspension with DNA was transferred to R-50 × 8 Multi-well Processing Assembly electroporation cuvettes. Cells were electro-porated using the manufacturer's High Energy A549 protocol and then allowed to recover for 30 min at 37°C before plating cells in Matrigel-coated dishes as described above. Seventy-two hours after electroporation, cells were sorted for mCherry fluorescence on a FACS Aria II flow cytometer (FACSDiva Software, BD Biosciences) at the UCSF Parnassus Flow Cytometry Core.

Lysosome pH measurements: For live-cell imaging of pHlys, cells were plated on Matrigel-coated 35-mm MatTek dishes (MatTek Corporation; P35G-1.5-10-C) for 48 h. For imaging pHLARE, fluorescence ratios (Ex488 for sfGFP and Ex561 for mCherry) from cells in growth medium were acquired over 1 min, followed by acquiring fluorescence ratios after 5 min each in a nigericin-containing buffer (50 mM KPO_4, 80 mM KCl, 1 mM MgCl) adjusted to 6.5 and 5.0 with HCl to calibrate ratios to pH values as previously described (Webb et al., 2021). Images were acquired using a customized spinning disk confocal (Yokogawa CSU-X1) on a Nikon Ti-E microscope with a 60X Plan TIRF 1.49 NA objective equipped with a Photometrics cMYO cooled CCD camera, as described (Stehbens et al., 2012). Lysosomal pH was also measured using ratiometric fluorescence imaging with the pH-sensitive dye Oregon Green 488 Dextran, 10,000 MW, Anionic, Lysine Fixable (Invitrogen, D7171), following previously described methods (Zhang et al., 2023). Twenty-four hours after plating, cells were washed, the medium was refreshed, and cells were incubated overnight with Oregon Green 488 at a concentration of 250 μg/ml. The next day, cells were washed three times and allowed a 3-h dye-free chase in fresh medium before fixing and imaging. Fluorescence emissions were collected at 530 nm with excitation wavelengths of 440 nm and 488 nm, respectively. After each imaging measurement, in situ pH calibration was performed by sequentially equilibrating cells with a series of pH-standard solutions for 5 min each, followed by imaging. The pH standards were prepared with 90 mM KCl, 25 mM MES, and 20 μM nigericin, adjusted to pH values of 4.1, 4.8, and 5.6, respectively. The ratio of fluorescence emission intensity of individual cells, acquired at excitation wavelengths of 488/440 nm after each pH treatment, was used to generate a standard curve, allowing the experimental fluorescence measurements to be interpolated into precise lysosomal pH values for each cell. Image acquisition settings that caused less than

5% photobleaching were used in all experiments. Images were analyzed using NIS Elements software and an analysis pipeline we developed as previously described (Webb et al., 2021). To determine lysosome size, we used the analysis pipeline program as previously described (Webb et al., 2021) that includes the area of lysosome objects. To evaluate the size of single lysosomes and not lysosome clusters, we used only the area of objects with a shape value between 0.9 and 1.0.

To experimentally change pHlys, 100 nM Bafilomycin A1 (Sigma-Aldrich; B1793) or 100 μM chloroquine (Sigma-Aldrich; C6628) was added to cells in growth medium for 2 h before pHLARE imaging, and 100 nM Torin-1 (Tocris Bioscience; 4247) or 10 μM DCPIB (Sigma-Aldrich; SML2692) was added to cells in growth medium for 24 h before pHLARE imaging as described above.

Intracellular pH measurements: Steady-state intracellular pH (pHi) was measured as previously described (Grillo-Hill et al., 2015; White et al., 2017). In brief, cells plated for 48 h in 24-well dishes were washed and incubated for 15 min in a $NaHCO_3$-containing buffer supplemented with 1 μM of the pH-sensitive dye BCECF. After washing in $NaHCO_3$-containing buffer, BCECF fluorescence ratios were measured using a Spectra-Max fluorescence plate reader (Molecular Devices) and calibrated to pHi by treating cells at the end of each measurement with a potassium phosphate buffer containing the protonophore nigericin (10 μM) at pH 6.5 and 7.5, as previously described (Grillo-Hill *et al.,* 2014). For measurements with DCPIB (10 μM), the inhibitor was added 24 h before pHi measurements and included in the BCECF-loading and pHi measurement buffers.

Lysosomal hydrolytic activity assay: The overall lysosomal hydrolytic activity was measured using DQ-Red BSA (Invitrogen, D12051). Cathepsin B activity was measured using the Magic Red Cathepsin B assay kit (ImmunoChemistry Technologies, #937). For both approaches, cells were plated on Matrigel-coated 35-mm MatTek dishes for 48 h and then incubated with DQ-Red BSA (10 μg/ml) at 37°C for 3 h or Magic Red (1:1000 dilution, following protocol instructions) at 37°C for 30 min, followed by washing three times with PBS. Images were acquired (λ_{exc}: 561 nm, λ_{em}: 628 nm) using spinning disk confocal microscopy as described above. NIS Elements software (Nikon) was used to analyze the images, which included fluorescence intensity with subtracted background fluorescence. For intensity measurements, fluorescence intensity was quantified from multiple regions of interest (ROIs) in the Z section with the highest intensity for each junction, using a maximum intensity projection. Intensity was calculated by collecting at least 30 different ROIs for each biological replicate. Data were normalized within each biological replicate to the mean intensity for all control values. Statistical two-way analyses of variance (ANOVA) were performed using Prism (GraphPad Software).

PROTEOSTAT Aggresome Detection Reagent: Protein aggregation was measured in cells plated for 48 h on Matrigel-coated 35-mm MatTek dishes. Cells were fixed in PBS containing 4% paraformaldehyde for 10 min at room temperature (RT), and after washing, were stained with 1/2000X diluted ProteoStat Aggresome Detection Kit (Enzo Life Sciences) according to the manufacturer's protocol and with Hoechst 33342 (1 mg/ml; Dojindo) to label nuclei for 30 min at room temperature in the dark. After washing with

PBS, images were acquired with a Nikon Ti-E microscope with a 60X Plan TIRF 1.49 NA objective equipped with a Photometrics cMYO cooled CCD camera and analyzed using ImageJ software. To experimentally change protein aggregation, 100 nM Bafilomycin A1 (Sigma-Aldrich; B1793) was added to cells in growth medium for 2 h before fixing.

Immunolabeling: Cells plated on Matrigel-coated 35-mm MatTek dishes for 48 h were washed 1X in PBS and fixed in PBS containing 4% paraformaldehyde for 10 min at RT. After washing with PBS, cells were permeabilized with 0.1% TritonX-100 in PBS for 10 min at RT, washed, and then incubated for 60 min in block buffer of PBS containing 5% FBS. Cells were then incubated with primary antibodies (Table 1) at 1:200 in PBS containing 0.01% Triton-X100 overnight at 4°C. After washing thrice with PBS, 10-min each wash, cells were incubated with fluorescence-conjugated secondary antibodies (1:200; Jackson ImmunoResearch Laboratories) in PBS for 60 min at RT and then washed three times with PBS, 10-min each wash. For Hoechst 33342 staining, dye (1:10,000) was added to the second PBS wash. Fluorescence images were acquired by spinning disk confocal microscopy as described for Proteostat staining and analyzed using NIS Elements software. For analysis of nuclear/cytoplasmic ratios, for each cell analyzed, mean fluorescence intensities were obtained from three drawn ROI in the cytoplasm and three ROI in the nucleus, the latter indicated by Hoechst staining.

Immunoblotting: Total lysates were obtained from cells plated on Matrigel-coated six well-plates for 48 h. Cells were washed three times in cold PBS on ice, lysed in 100 µl/well RIPA buffer (50 mM Tris-HCL, 150 mM NaCl, 1 mM EDTA, 1% NP-40, 0.5% deoxycholate, 0.1% SDS supplemented with protease inhibitors PEFA) while rotating at 4°C for 10 min, scrapped into microfuge tubes, and a postnuclear supernatant was collected after centrifugation at 12,000 rpm for 5 min at 4°C. Proteins in lysates were separated by SDS–PAGE and transferred to polyvinylidene difluoride membranes. The membranes were incubated in blocking buffer (TBS containing 0.1% Tween [TBSTw] containing 5% BSA or 5% non-fat milk for 1 h and then incubated with primary antibodies (Table 1; 1:1000 dilution in TB-STw) overnight at 4°C. After washing, membranes were incubated with peroxidase—conjugated secondary antibodies (Jackson ImmunoResearch Laboratories) in TBSTw for 1 h at RT, and bound antibodies were developed by enhanced chemiluminescence using SuperSignal West Femto (Thermo Fisher Scientific) and imaged using an Alpha Innotech FluorChem Q (Alpha Innotech). Images were analyzed using ImageJ software. Immunoblots were performed using samples from at least three independent cell preparations, with actin or vinculin serving as a loading control. Quantification is presented as mean ± SEM, based on data from at least three separate cell preparations, and statistical significance was determined using Studen's *t* test.

RNA sequencing: RNA was extracted from iPSCs plated for 48 h on a Matrigel-coated 6 WP with the RNAeasy Micro Kit (Qiagen #74004) according to the manufacturer's protocol with the following modifications: after disrupting the cells with RLT buffer, the cell suspension was transferred into a QIAshredder spin column (Qiagen #79656) and centrifuged. The lysate was transferred to a QIAshredder spin column and centrifuged at 13,000 rpm for 2 min. The RNA concentration and purity were measured using SpectraMax

QuickDrop UV-Vis Spectrophotometer (Molecular Devices, #7546). Libraries were prepared with the RNA Library Prep Kit (Illumina), and paired-end sequencing was completed using the NovaSeq 6000 (Illumina) with 3 samples/lane. The raw RNA-Seq reads were analyzed by Novogene (Beijing, China). Functional enrichment analysis of differentially expressed genes was performed using GO and Kyoto Encyclopedia of Genes and Genomes (KEGG) pathway analysis. The results were visualized using R packages such as ggplot2.

Data presentation and statistical analysis: Sample sizes and *p* values were reported in the corresponding figure legends. Box-and-whisker plots were generated using Analyse-It for Microsoft Excel and show median, first, and third quartiles, observations within 1.5 times the interquartile range, and all individual data points. Scatter dot plots and statistical analyses were generated in GraphPad Prism 10. Data distribution was tested to be normal. Unless otherwise noted, graphs show mean ± SEM. Statistical significance was determined using either statistical analysis by Tukey–Kramer HSD, two-way ANOVA, or unpaired *t* test. Images were representative of at least three independent experiments. Experiments were not randomized, and the investigators were not blinded during data analysis.

Supplementary Material

Refer to Web version on PubMed Central for supplementary material.

ACKNOWLEDGMENTS

This work was supported by awards from the Alliance for Therapeutics in Neuroscience (ATN), Genentech (no. 4301), and the National Institutes of Health (NIH CA-197855).

Data and code availability

RNA-seq data generated during this study have been deposited in Gene Expression Omnibus (https://www.ncbi.nlm.nih.gov/geo/). The accession number for the data reported in this paper is Gene Expression Omnibus GSE273025. The overall project RNA-seq raw data are available for public download in the NCBI database under accession code PRJNA1121636. Software/packages used to analyze the dataset were freely available.

Abbreviations used:

AD	Alzheimer’s disease
ALS	amyotrophic lateral sclerosis
ANXA2	annexin 2
CNTFR	ciliary neurotrophic factor receptor
DCPIB	4-(2-(6,7-Dichloro-2-cyclopentylindan-1-on-5-yl)ethyl)benzene-1,3-diol
FTD	frontotemporal dementia
GRN	progranulin

iPSCs	induced pluripotent stem cells
LAMP1	lysosomal associated membrane protein 1
MSN	moesin
mTORC1	mammalian target of rapamycin complex 1
NINDS	National Institute of Neurological Disorders and Stroke
pHi	intracellular (cytosolic) pH
pHlys	lysosomal pH
PD	Parkinson’s disease
TDP-43	TAR DNA-binding protein 43
TMEM175	transmembrane protein 175

REFERENCES

Ahmed M, Spicer C, Harley J, Taylor JP, Hanna M, Patani R, Greensmith L (2023). Amplifying the heat shock response ameliorates ALS and FTD pathology in mouse and human models. Mol Neurobiol 60, 6896–6915. [PubMed: 37516663]

Almansoub H, Tang H, Wu Y, Wang D-Q, Mahaman YAR, Wei N, Almansob YA, He W, Liu D (2019). Tau abnormalities and the potential therapy in Alzheimer’s disease. J Alzheimers Dis 67, 13–33. [PubMed: 30507581]

Amick J, Ferguson SM (2017). C9orf72: At the intersection of lysosome cell biology and neurodegenerative disease. Traffic 18, 267–276. [PubMed: 28266105]

Babić Leko M, Župunski V, Kirincich J, Smilović D, Hortobágyi T, Hof PR, šimić G (2019). Molecular mechanisms of neurodegeneration related to C9ort72 hexanucleotide repeat expansion. Behav Neurol 2019, 2909168. [PubMed: 30774737]

Bandyopadhyay D, Cyphersmith A, Zapata JA, Kim YJ, Payne CK (2014). Lysosome transport as a function of lysosome diameter. PLoS One 9, e86847. [PubMed: 24497985]

Beckers J, Tharkeshwar AK, Fumagalli L, Contardo M, Van Sbhoor E, Fazal R, Thal DR, Chandran S, Manbuso R, Van Den Bosbh L, Van Damme P (2023). A toxic gain-of-function mechanism in C9orf72 ALS impairs the autophagy-lysosome pathway in neurons. Acta Neuropathol Commun 11, 151. [PubMed: 37723585]

Beckers J, Van Damme P (2024). Toxib gain-of-funbtion mebhanisms in *C9orf72* ALS-FTD neurons drive autophagy and lysosome dysfunction. Autophagy 20, 2102–2104. [PubMed: 38615685]

Beckmann A, Ramirez P, Gamez M, Gonzalez E, De Mange J, Bieniek KF, Ray WJ, Frost B (2023). Moesin is an effector of tau-induced actin overstabilization, cell cycle activation, and neurotoxicity in Alzheimer’s disease. iScience 26, 106152. [PubMed: 36879821]

Canton J, Grinstein S (2017). Measuring phagosomal pH by fluorescence microscopy. In: Botelho R (ed.) Phagocytosis and Phagosomes: Methods and Protocols, Methods in Molecular Biology, vol. 1519. New York, NY: Springer, pp. 185–199.

Casey JR, Grinstein S, Orlowski J (2010). Sensors and regulators of intracellular pH. Nat Rev Mol Cell Biol 11,50–61. [PubMed: 19997129]

Chang C-C, Li H-H, Tsou S-H, Hung H-C, Liu G-Y, Korolenko TA, Lai T-J, Ho Y-J, Lin C-L (2020). The pluripotency factor nanog protects against neuronal amyloid beta-induced toxicity and oxidative stress through insulin sensitivity restoration. Cells 9, 1339. [PubMed: 32471175]

Chew J, Gendron TF, Prudencio M, Sasaguri H, Zhang YJ, Castanedes-Casey M, Lee CW, Jansen-West K, Kurti A, Murray ME, Bieniek KF, et al. . (2015) Neurodegeneration. C9ORF72 repeat

expansions in mice cause TDP-43 pathology, neuronal loss, and behavioral deficits. Science 348, 1151–1154. [PubMed: 25977373]

Chin MY, Ang K-H, Davies J, Alquezar C, Garda VG, Rooney B, Leng K, Kampmann M, Arkin MR, Kao AW (2022). Phenotypic screening using high-content imaging to identify lysosomal ph modulators in a neuronal cell model. ACS Chem Neurosci 13, 1505–1516. [PubMed: 35522480]

Cho S, Hwang ES (2012). Status of mTOR activity may phenotypically differentiate senescence and quiescence. Mol Cells 33, 597–604. [PubMed: 22570149]

Colacurcio DJ, Nixon RA (2016). Disorders of lysosomal acidification-The emerging role of v-ATPase in aging and neurodegenerative disease. Ageing Res Rev 32, 75–88. [PubMed: 27197071]

Coppola MA, Tettey-Matey A, Imbrici P, Gavazzo P, Liantonio A, Pusch M (2023). Biophysical aspects of neurodegenerative and neurodevelopmental disorders involving endo-/lysosomal CLC Cl(−)/H(+) antiporters. Life (Basel) 13, 1317. [PubMed: 37374100]

Czuppa M, Dhingra A, Zhou Q, Schludi C, König L, Scharf E, Farny D, Dalmia A, Täger J, Castillo-Lizardo M, Katona E, et al. (2022). Drug screen in iPSC-Neurons identifies nucleoside analogs as inhibitors of (G4C2)n expression in C9orf72 ALS/FTD. Cell Rep 39, 110913. [PubMed: 35675776]

de Araujo MEG, Liebscher G, Hess MW, Huber LA (2020). Lysosomal size matters. Traffic 21, 60–75. [PubMed: 31808235]

Decher N, Lang HJ, Nilius B, Brüggemann A, Busch AE, Steinmeyer K (2001). DCPIB is a novel selective blocker of I(Cl,swell) and prevents swelling-induced shortening of guinea-pig atrial action potential duration. Br J Pharmacol 134, 1467–1479. [PubMed: 11724753]

DeJesus-Hernandez M, Mackenzie IR, Boeve BF, Boxer AL, Baker M, Rutherford NJ, Nicholson AM, Finch NA, Flynn H, Adamson J, Kouri N, et al. (2011). Expanded GGGGCC hexanucleotide repeat in noncoding region of C9ORF72 causes chromosome 9p-linked FTD and ALS. Neuron 72, 245–256. [PubMed: 21944778]

Deolankar SC, Patil AH, Rex DAB, Subba P, Mahadevan A, Prasad TSK (2021). Mapping post-translational modifications in brain regions in Alzheimer's disease using proteomics data mining. OMICS 25, 525–536. [PubMed: 34255573]

Duan Z, Zhang S, Liang H, Xing Z, Guo L, Shi L, Du L, Kuang C, Takikawa O, Yang Q (2020). Amyloid β neurotoxicity is IDO1-Kyn-AhR dependent and blocked by IDO1 inhibitor. Signal Transduct Target Ther 5, 96. [PubMed: 32532956]

Elia L, Herting B, Alijagic A, Buselli C, Wong L, Morrison G, Prado MA, Paulo JA, Gygi SP, Finley D, Finkbeiner S (2023). Frontotemporal dementia patient neurons with progranulin deficiency display protein dyshomeostasis. bioRxiv (Preprint), 10.1101/2023.01.18.524611.

Esanov R, Belle KC, van Blitterswijk M, Belzil VV, Rademakers R, Dickson DW, Petrucelli L, Boylan KB, Dykxhoorn DM, Wuu J, Benatar M, et al. (2016) C9orf72 promoter hypermethylation is reduced while hydroxymethylation is acquired during reprogramming of ALS patient cells. Exp Neurol 277, 171–177. [PubMed: 26746986]

Espuny-Camacho I, Michelsen KA, Gall D, Linaro D, Hasche A, Bonnefont J, Bali C, Orduz D, Bilheu A, Herpoel A, Lambert N, et al. (2013). Pyramidal neurons derived from human pluripotent stem cells integrate efficiently into mouse brain circuits in vivo. Neuron 77, 440–456. [PubMed: 23395372]

Fang B, Wang D, Huang M, Yu G, Li H (2010). Hypothesis on the relationship between the change in intracellular pH and incidence of sporadic Alzheimer's disease or vascular dementia. Int J Neurosci 120, 591–595. [PubMed: 20707633]

Farg MA, Sundaramoorthy V, Sultana JM, Yang S, Atkinson RA, Levina V, Halloran MA, Gleeson PA, Blair IP, Soo KY, et al. (2014). C9ORF72, implicated in amytrophic lateral sclerosis and frontotemporal dementia, regulates endosomal trafficking. Hum Mol Genet 23, 3579–3595. [PubMed: 24549040]

Gersten M, Alirezaei M, Marcondes MC, Flynn C, Ravasi T, Ideker T, Fox HS (2009). An integrated systems analysis implicates EGR1 downregulation in simian immunodeficiency virus encephalitis-induced neural dysfunction. J Neurosci 29, 12467–12476. [PubMed: 19812322]

Graves AR, Curran PK, Smith CL, Mindell JA (2008). The Cl−/H+ antiporter ClC-7 is the primary chloride permeation pathway in lysosomes. Nature 453, 788–792. [PubMed: 18449189]

Greaves CV, Rohrer JD (2019). An update on genetic frontotemporal dementia. J Neurol 266, 2075–2086. [PubMed: 31119452]

Grewal T, Gerke V, Nylandsted J, Rentero C, Enrich C (2025). Revisiting the role of Annexins in membrane trafficking. Cell Mol Life Sci 82, 230. [PubMed: 40506619]

Grillo-Hill BK, Choi C, Jimenez-Vidal M, Barber DL (2015). Increased H^+ efflux is sufficient to induce dysplasia and necessary for viability with oncogene expression. Elife 4, e03270. [PubMed: 25793441]

Hadi F, Mortaja M, Hadi Z (2024). Calcium (Ca^{2+}) hemostasis, mitochondria, autophagy, and mitophagy contribute to Alzheimer's disease as early moderators. Cell Biochem Funct 42, e4085. [PubMed: 38951992]

Halcrow PW, Geiger JD, Chen X (2021). Overcoming chemoresistance: Altering pH of cellular compartments by chloroquine and hydroxychloroquine. Front Cell Dev Biol 9, 627639. [PubMed: 33634129]

Halliday GM, Holton JL, Revesz T, Dickson DW (2011). Neuropathology underlying clinical variability in patients with synucleinopathies. Acta Neuropathol 122, 187–204. [PubMed: 21720849]

Hu M, Li P, Wang C, Feng X, Geng Q, Chen W, Marthi M, Zhang W, Gao C, Reid W, et al. (2022). Parkinson's disease-risk protein TMEM175 is a proton-activated proton channel in lysosomes. Cell 185, 2292–2308.e20. [PubMed: 35750034]

Hu M, Zhou N, Cai W, Xu H (2022). Lysosomal solute and water transport. J Cell Biol 221, e202109133. [PubMed: 36219209]

Hung S-T, Linares GR, Chang W-H, Eoh Y, Krishnan G, Mendonca S, Hong S, Shi Y, Santana M, Kueth C, et al. (2023). PIKFYVE inhibition mitigates disease in models of diverse forms of ALS. Cell 186, 786–802.e28. [PubMed: 36754049]

Imai Y, Meng H, Shiba-Fukushima K, Hattori N (2019). Twin CHCH proteins, CHCHD2, and CHCHD10: Key molecules of Parkinson's disease, amyotrophic lateral sclerosis, and frontotemporal dementia. Int J Mol Sci 20, 908. [PubMed: 30791515]

Irwin DJ, Cairns NJ, Grossman M, McMillan CT, Lee EB, Van Deerlin VM, Lee VMY, Trojanowski JQ (2015). Frontotemporal lobar degeneration: defining phenotypic diversity through personalized medicine. Acta Neuropathol 129, 469–491. [PubMed: 25549971]

Jain V, Bose S, Arya AK, Arif T (2022). Lysosomes in stem cell quiescence: A potential therapeutic target in acute myeloid leukemia. Cancers (Basel) 14, 1618. [PubMed: 35406389]

Kos J, Mitrović A, Perišić Nanut M, Pišlar A (2022). Lysosomal peptidases—intriguing roles in cancer progression and neurodegeneration. FEBS Open Bio 12, 708–738.

Lara Flores E, Qi A, Reilly L, Santiana M, Ward M, Cookson M. (2023). iNDI Transcription Factor-NGN2 differentiation of human iPSC into cortical neurons Version. 2. 83415, 10.17504/protocols.io.n2bvj3owblk5/v1.

Lee J-H, Yu WH, Kumar A, Lee S, Mohan PS, Peterhoff CM, Wolfe DM, Martinez-Vicente M, Massey AC, Sovak G, et al. (2010). Lysosomal proteolysis and autophagy require presenilin 1 and are disrupted by Alzheimer-related PS1 mutations. Cell 141, 1146–1158. [PubMed: 20541250]

Lee S, Huang EJ (2017). Modeling ALS and FTD with iPSC-derived neurons. Brain Res 1656, 88–97. [PubMed: 26462653]

Levine B, Kroemer G (2008). Autophagy in the pathogenesis of disease. Cell 132, 27–42. [PubMed: 18191218]

Liao YZ, Ma J, Dou JZ (2022). The role of TDP-43 in neurodegenerative disease. Mol Neurobiol 59, 4223–4241. [PubMed: 35499795]

Lines G, Casey JM, Preza E, Wray S (2020). Modelling frontotemporal dementia using patient-derived induced pluripotent stem cells. Mol Cell Neurosci 109, 103553. [PubMed: 32956830]

Ling SC, Polymenidou M, Cleveland DW (2013). Converging mechanisms in ALS and FTD: disrupted RNA and protein homeostasis. Neuron 79, 416–438. [PubMed: 23931993]

Lo CH, Zeng J (2023). Defective lysosomal acidification: a new prognostic marker and therapeutic target for neurodegenerative diseases. Transl Neurodegener 12, 29. [PubMed: 37287072]

Lopez-Herdoiza M-B, Bauché S, Wilmet B, Le Duigou C, Roussel D, Frah M, Béal J, Devely G, Boluda S, Frick P, et al. (2023). C9ORF72 knockdown triggers FTD-like symptoms and cell pathology in mice. Front Cell Neurosci 17, 1155929. [PubMed: 37138765]

Majdi A, Mahmoudi J, Sadigh-Eteghad S, Golzari SE, Sabermarouf B, Reyhani-Rad S (2016). Permissive role of cytosolic pH acidification in neurodegeneration: A closer look at its causes and consequences. J Neurosci Res 94, 879–887. [PubMed: 27282491]

Marian OC, Teo JD, Lee JY, Song H, Kwok JB, Landin-Romero R, Halliday G, Don AS (2023). Disrupted myelin lipid metabolism differentiates frontotemporal dementia caused by GRN and C9orf72 gene mutations. Acta Neuropathol Commun 11, 52. [PubMed: 36967384]

Mizielinska S, Grönke S, Niccoli T, Ridler CE, Clayton EL, Devoy A, Moens T, Norona FE, Woollacott IO, Pietrzyk J, et al. (2014). C9orf72 repeat expansions cause neurodegeneration in Drosophila through arginine-rich proteins. Science 345, 1192–1194. [PubMed: 25103406]

Mutvei AP, Nagiec MJ, Blenis J (2023). Balancing lysosome abundance in health and disease. Nat Cell Biol 25, 1254–1264. [PubMed: 37580388]

Neumann M, Mackenzie IRA. (2019). Review: Neuropathology of non-tau frontotemporal lobar degeneration. Neuropathol Appl Neurobiol 45, 19–40. [PubMed: 30357887]

Neumann M, Sampathu DM, Kwong LK, Truax AC, Micsenyi MC, Chou TT, Bruce J, Schuck T, Grossman M, Clark CM, et al. (2006). Ubiquitinated TDP-43 in frontotemporal lobar degeneration and amyotrophic lateral sclerosis. Science 314, 130–133. [PubMed: 17023659]

Nixon RA (2017). Amyloid precursor protein and endosomal-lysosomal dysfunction in Alzheimer's disease: Inseparable partners in a multifactorial disease. FASEB J 31, 2729–2743. [PubMed: 28663518]

Nixon RA (2020). The aging lysosome: An essential catalyst for late-onset neurodegenerative diseases. Biochim Biophys Acta Proteins Proteom 1868, 140443. [PubMed: 32416272]

Ojalvo-Pacheco J, Yakhine-Diop SMS, Fuentes JM, Paredes-Barquero M, Niso-Santano M (2024). Role of TFEB in Huntington's disease. Biology (Basel) 13, 238. [PubMed: 38666850]

Pan S, Chen R, Tamura Y, Crispin DA, Lai LA, May DH, McIntosh MW, Goodlett DR, Brentnall TA (2014). Quantitative glycoproteomics analysis reveals changes in N-glycosylation level associated with pancreatic ductal adenocarcinoma. J Proteome Res 13, 1293–1306. [PubMed: 24471499]

Paquette M, El-Houjeiri L, L CZ, Puustinen P, Blanchette P, Jeong H, Dejgaard K, Siegel PM, Pause A (2021). AMPK-dependent phosphorylation is required for transcriptional activation of TFEB and TFE3. Autophagy 17, 3957–3975. [PubMed: 33734022]

Podvin S, Jiang Z, Boyarko B, Rossitto L-A, O'Donoghue A, Rissman RA, Hook V (2022). Dysregulation of neuropeptide and tau peptide signatures in human Alzheimer's disease brain. ACS Chem Neurosci 13,19922005.

Qi Y, Zhang XJ, Renier N, Wu Z, Atkin T, Sun Z, Ozair MZ, Tchieu J, Zimmer B, Fattahi F, et al. (2017). Combined small-molecule inhibition accelerates the derivation of functional cortical neurons from human pluripotent stem cells. Nat Biotechnol 35, 154–163. [PubMed: 28112759]

Quick JD, Silva C, Wong JH, Lim KL, Reynolds R, Barron AM, Zeng J, Lo CH (2023). Lysosomal acidification dysfunction in microglia: an emerging pathogenic mechanism of neuroinflammation and neurodegeneration. J Neuroinflammation 20, 185. [PubMed: 37543564]

Rademakers R, Neumann M, Mackenzie IR (2012). Advances in understanding the molecular basis of frontotemporal dementia. Nat Rev Neurol 8, 423–434. [PubMed: 22732773]

Raitano S, Ordovas L, De Muynck L, Guo W, Espuny-Camacho I, Geraerts M, Khurana S, Vanuytsel K, Toth BI, Voets T, et al. (2015). Restoration of progranulin expression rescues cortical neuron generation in an induced pluripotent stem cell model of frontotemporal dementia. Stem Cell Reports 4, 16–24. [PubMed: 25556567]

Ratti A, Gumina V, Lenzi P, Bossolasco P, Fulceri F, Volpe C, Bardelli D, Pregnolato F, Maraschi A, Fornai F, et al. (2020). Chronic stress induces formation of stress granules and pathological TDP-43 aggregates in human ALS fibroblasts and iPSC-motoneurons. Neurobiol Dis 145, 105051. [PubMed: 32827688]

Rentero C, Blanco-Munoz P, Meneses-Salas E, Grewal T, Enrich C (2018). Annexins-coordinators of cholesterol homeostasis in endocytic pathways. Int J Mol Sci 19, 1444. [PubMed: 29757220]

Renton AE, Majounie E, Waite A, Simon-Sanchez J, Rollinson S, Gibbs JR, Schymick JC, Laaksovirta H, Van Swieten JC, Myllykangas L, et al. (2011). A hexanucleotide repeat expansion in C9ORF72 is the cause of chromosome 9p21-linked ALS-FTD. Neuron 72, 257–268. [PubMed: 21944779]

Rojas-Prats E, Martinez-Gonzalez L, Gonzalo-Consuegra C, Liachko NF, Perez C, Ramirez D, Kraemer BC, Martin-Requero A, Perez DI, Gil C, et al. (2021). Targeting nuclear protein TDP-43 by cell division cycle kinase 7 inhibitors: A new therapeutic approach for amyotrophic lateral sclerosis. Eur J Med Chem 210, 112968. [PubMed: 33139113]

Root J, Merino P, Nuckols A, Johnson M, Kukar T (2021). Lysosome dysfunction as a cause of neurodegenerative diseases: Lessons from frontotemporal dementia and amyotrophic lateral sclerosis. Neurobiol Dis 154, 105360. [PubMed: 33812000]

Sardini A, Amey JS, Weylandt KH, Nobles M, Valverde MA, Higgins CF (2003). Cell volume regulation and swelling-activated chloride channels. Biochim BiophysActa 1618, 153–162.

Sathe G, Albert M, Darrow J, Saito A, Troncoso J, Pandey A, Moghekar A (2021). Quantitative proteomic analysis of the frontal cortex in Alzheimer's disease. J Neurochem 156, 988–1002. [PubMed: 32614981]

Selvaraj BT, Livesey MR, Chandran S (2017). Modeling the C9ORF72 repeat expansion mutation using human induced pluripotent stem cells. Brain Pathol 27, 518–524. [PubMed: 28585384]

Seredenina T, Gokce O, Luthi-Carter R (2011). Decreased striatal RGS2 expression is neuroprotective in Huntington's disease (HD) and exemplifies a compensatory aspect of HD-induced gene regulation. PLoS One 6, e22231. [PubMed: 21779398]

Shao W, Todd TW, Wu Y, Jones CY, Tong J, Jansen-West K, Daughrity LM, Park J, Koike Y, Kurti A, et al. (2022). Two FTD-ALS genes converge on the endosomal pathway to induce TDP-43 pathology and degeneration. Science 378, 94–99. [PubMed: 36201573]

Shariq M, Khan MF, Raj R, Ahsan N, Kumar P (2024). PRKAA2, MTOR, and TFEB in the regulation of lysosomal damage response and autophagy. J Mol Med (Berl) 102, 287–311. [PubMed: 38183492]

Shaw MP, Higginbottom A, McGown A, Castelli LM, James E, Hautbergue GM, Shaw PJ, Ramesh TM (2018). Stable transgenic C9orf72 zebrafish model key aspects of the ALS/FTD phenotype and reveal novel pathological features. Acta Neuropathol Commun 6, 125. [PubMed: 30454072]

Shi Y, Lin S, Staats KA, Li Y, Chang W-H, Hung S-T, Hendricks E, Linares GR, Wang Y, Son EY, et al. (2018). Haploinsufficiency leads to neurodegeneration in C9ORF72 ALS/FTD human induced motor neurons. Nat Med 24,313–325. [PubMed: 29400714]

Siddiqui T, Bhatt LK (2024). Emerging autophagic endo-lysosomal targets in the management of Parkinson's disease. Rev Neurol 180, 477–485, 10.1016/j.neurol.2023.07.007. [PubMed: 37586941]

Smeele PH, Cesare G, Vaccari T (2024). ALS' perfect storm: *C9orf72*-associated toxic dipeptide repeats as potential multipotent disruptors of protein homeostasis. Cells 13, 178. [PubMed: 38247869]

Smith JR, Maguire S, Davis LA, Alexander M, Yang F, Chandran S, Ffrench-Constant C, Pedersen RA (2008). Robust, persistent transgene expression in human embryonic stem cells is achieved with AAVS1-targeted integration. Stem Cells 26, 496–504. [PubMed: 18024421]

Sonobe Y, Lee S, Krishnan G, Gu Y, Kwon DY, Gao FB, Roos RP, Kratsios P (2023). Translation of dipeptide repeat proteins in *C90RF72* ALS/FTD through unique and redundant AUG initiation codons. Elife 12, e83189. [PubMed: 37675986]

Stehbens S, Pemble H, Murrow L, Wittmann T (2012). Imaging intracellular protein dynamics by spinning disk confocal microscopy. Methods Enzymol 504, 293–313. [PubMed: 22264541]

Südhof TC (2012). Calcium control of neurotransmitter release. Cold Spring Harb Perspect Biol 4, a011353. [PubMed: 22068972]

Swift IJ, Sjodin S, Gobom J, Brinkmalm A, Blennow K, Zetterberg H, Rohrer JD, Sogorb-Esteve A (2024). Differential patterns of lysosomal dysfunction are seen in the clinicopathological forms of primary progressive aphasia. J Neurol 271, 1277–1285. [PubMed: 37917233]

Tanaka Y, Ito SI, Honma Y, Hasegawa M, Kametani F, Suzuki G, Kozuma L, Takeya K, Eto M (2023). Dysregulation of the progranulin-driven autophagy-lysosomal pathway mediates secretion of the nuclear protein TDP-43. J Biol Chem 299, 105272. [PubMed: 37739033]

Tanaka Y, Suzuki G, Matsuwaki T, Hosokawa M, Serrano G, Beach TG, Yamanouchi K, Hasegawa M, Nishihara M (2017). Progranulin regulates lysosomal function and biogenesis through acidification of lysosomes. Hum Mol Genet 26, 969–988. [PubMed: 28073925]

Tang T, Jian B, Liu Z (2023). Transmembrane protein 175, a lysosomal ion channel related to Parkinson's disease. Biomolecules 13, 802. [PubMed: 37238672]

Taylor JP, Hardy J, Fischbeck KH (2002). Toxic proteins in neurodegenerative disease. Science 296, 1991–1995. [PubMed: 12065827]

Thoreen CC, Kang SA, Chang JW, Liu Q, Zhang J, Gao Y, Reichling LJ, Sim T, Sabatini DM, Gray NS (2009). An ATP-competitive mammalian target of rapamycin inhibitor reveals rapamycin-resistant functions of mTORC1. J Biol Chem 284, 8023–8032. [PubMed: 19150980]

Thwaites DT, Anderson CM (2011). The SLC36 family of proton-coupled amino acid transporters and their potential role in drug transport. Br J Pharmacol 164, 1802–1816. [PubMed: 21501141]

Todd TW, Shao W, Zhang YJ, Petrucelli L (2023). The endolysosomal pathway and ALS/FTD. Trends Neurosci 46, 1025–1041. [PubMed: 37827960]

Tu C, Ortega-Cava CF, Chen G, Fernandes ND, Cavallo-Medved D, Sloane BF, Band V, Band H (2008). Lysosomal cathepsin B participates in the podosome-mediated extracellular matrix degradation and invasion via secreted lysosomes in v-Src fibroblasts. Cancer Res 68, 9147–9156. [PubMed: 19010886]

Ugolino J, Ji YJ, Conchina K, Chu J, Nirujogi RS, Pandey A, Brady NR, Hamacher-Brady A, Wang J (2016). Loss of C9orf72 enhances autophagic activity via deregulated mTOR and TFEB signaling. PLoS Genet 12, e1006443. [PubMed: 27875531]

Valdez C, Wong YC, Schwake M, Bu G, Wszolek ZK, Krainc D (2017). Progranulin-mediated deficiency of cathepsin D results in FTD and NCL-like phenotypes in neurons derived from FTD patients. Hum Mol Genet 26, 4861–4872. [PubMed: 29036611]

Vo QD, Saito Y, Ida T, Nakamura K, Yuasa S (2024). The use of artificial intelligence in induced pluripotent stem cell-based technology over 10-year period: A systematic scoping review. PLoS One 19, e0302537. [PubMed: 38771829]

Wang F, Gomez-Sintes R, Boya P (2018). Lysosomal membrane permeabilization and cell death. Traffic 19, 918–931. [PubMed: 30125440]

Wang H, Wang R, Xu S, Lakshmana MK (2016). Transcription factor EB is selectively reduced in the nuclear fractions of Alzheimer's and amyotrophic lateral sclerosis brains. Neurosci J 2016, 4732837. [PubMed: 27433468]

Wang M, Wang H, Tao Z, Xia Q, Hao Z, Prehn JHM, Zhen X, Wang G, Ying Z (2020). C9orf72 associates with inactive Rag GTPases and regulates mTORC1-mediated autophagosomal and lysosomal biogenesis. Aging Cell 19, e13126. [PubMed: 32100453]

Webb BA, Aloisio FM, Charafeddine RA, Cook J, Wittmann T, Barber DL (2021). pHLARE: a new biosensor reveals decreased lysosome pH in cancer cells. Mol Biol Cell 32, 131–142. [PubMed: 33237838]

White AJ, Clark KA, Alexander KD, Ramalingam N, Young-Pearse TL, Dettmer U, Selkoe DJ, Ho GP (2024). A stem cell-based assay platform demonstrates alpha-synuclein dependent synaptic dysfunction in patient-derived cortical neurons. NPJ Parkinsons Dis 10, 107. [PubMed: 38773105]

White KA, Grillo-Hill BK, Barber DL (2017). Cancer cell behaviors mediated by dysregulated pH dynamics at a glance. J Cell Sci 130, 663–669. [PubMed: 28202602]

Wolfe DM, Lee JH, Kumar A, Lee S, Orenstein SJ, Nixon RA (2013). Autophagy failure in Alzheimer's disease and the role of defective lysosomal acidification. Eur J Neurosci 37, 1949–1961. [PubMed: 23773064]

Xu G, Peng H, Yao R, Yang Y, Li B (2024). TFEB and TFE3 cooperate in regulating inorganic arsenic-induced autophagy-lysosome impairment and immuno-dysfunction in primary dendritic cells. Cell Biol Toxicol 40, 4. [PubMed: 38267572]

Yong J, Groeger S, von Bremen J, Ruf S (2022). Ciliary neurotrophic factor (CNTF) and its receptors signal regulate cementoblasts apoptosis through a mechanism of ERK1/2 and caspases signaling. Int J Mol Sci 23, 8335. [PubMed: 35955469]

Zhang J, Zeng W, Han Y, Lee W-R, Liou J, Jiang Y (2023). Lysosomal LAMP proteins regulate lysosomal pH by direct inhibition of the TMEM175 channel. Mol Cell 83, 2524–2539.e7. [PubMed: 37390818]

Zou HY, Guo L, Zhang B, Chen S, Wu XR, Liu XD, Xu XY, Li BY, Chen S, Xu NJ, Sun S (2022). Aberrant miR-339-5p/neuronatin signaling causes prodromal neuronal calcium dyshomeostasis in mutant presenilin mice. J Clin Invest 132, e149160. [PubMed: 35426376]

SIGNIFICANCE STATEMENT

Understanding the cellular pathology of frontotemporal dementia linked to a GGGGCC expansion in the C9orf72 gene remains a challenge.

This study shows that undifferentiated patient-derived iPSCs exhibit hallmark FTD characteristics, including lysosome dysfunction and TDP-43 proteinopathy, and identifies dysregulated genes related to neurodegeneration.

These findings highlight patient-derived iPSCs as a valuable model for studying FTD pathology and for drug screening, potentially guiding future research in therapeutic development.

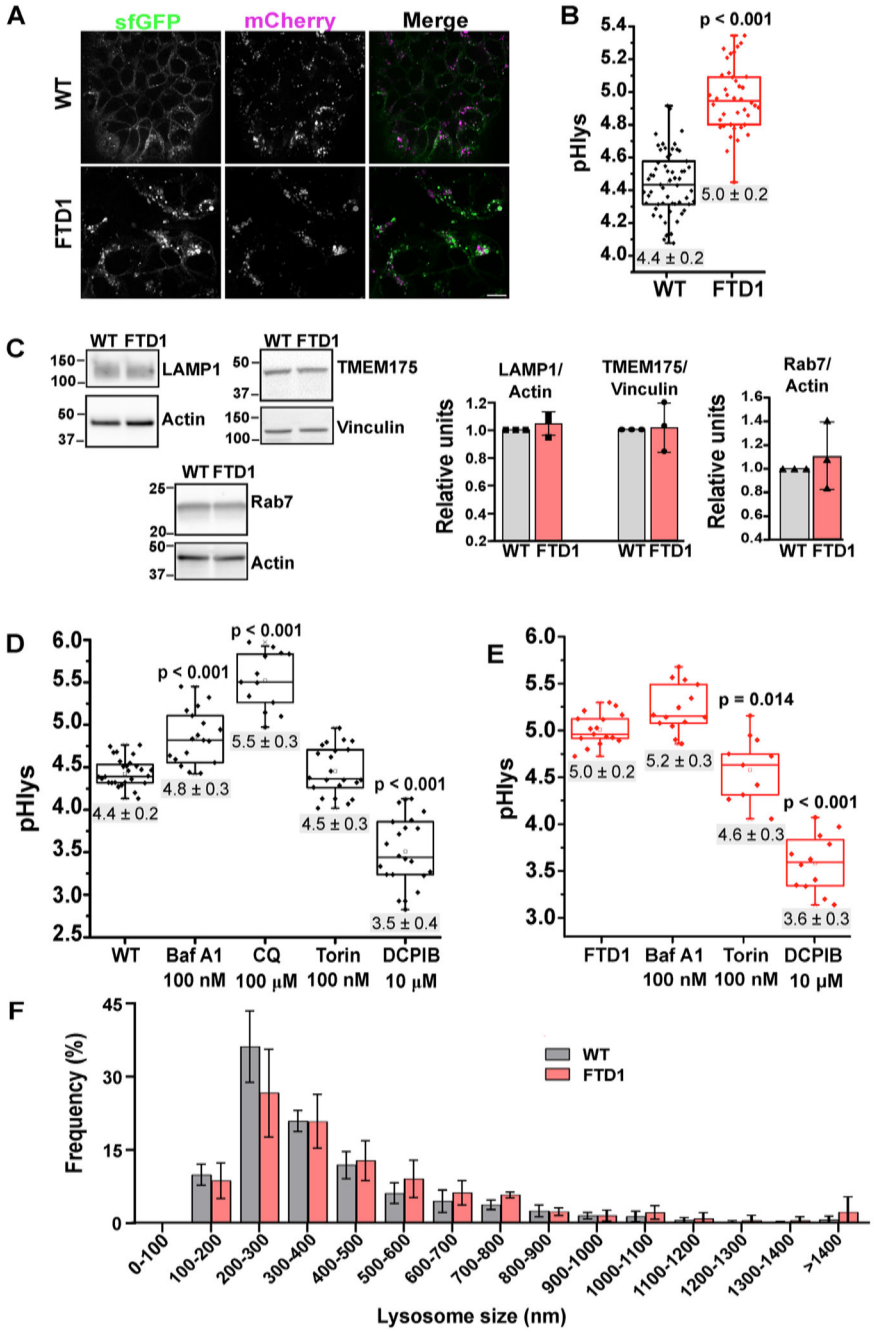

FIGURE 1:

Lysosome characteristics in FTD iPSCs. (A) Confocal images of wild-type (WT) and frontotemporal dementia (FTD) induced pluripotent stem cells (iPSCs) expressing pHLARE, showing superfolder (sfGFP), mCherry, and merged fluorescence signals. Scale bar 15 µm. (B) Quantified pHlys in WT and FTD1 iPSCs obtained from pHLARE sfGFP/ mCherry ratios calibrated with nigericin-containing buffers of known pH values. Box plots show median, first, and third quartile, with whiskers extending to observations within 1.5 times the interquartile range, with data points indicating individual cells (WT 60 cells;

FTD1 45 cells) obtained from 5 separate cell preparations. Statistical analysis by Dunnett's multiple comparison test. (C) Representative immunoblots and quantified data from three separate cell preparations for abundance of TMEM175, LAMP1, and Rab7 in lysates of WT and FTD1 iPSC normalized to loading controls of either vinculin or actin (D and E) The pHlys of WT (D) and FTD (E) iPSCs after treatment with different chemical reagents. Data were expressed as described in (B) and obtained from three separate cell preparations. (F) Lysosome size determined by measuring ca. 1000 lysosomes per cell line in four cell preparations.

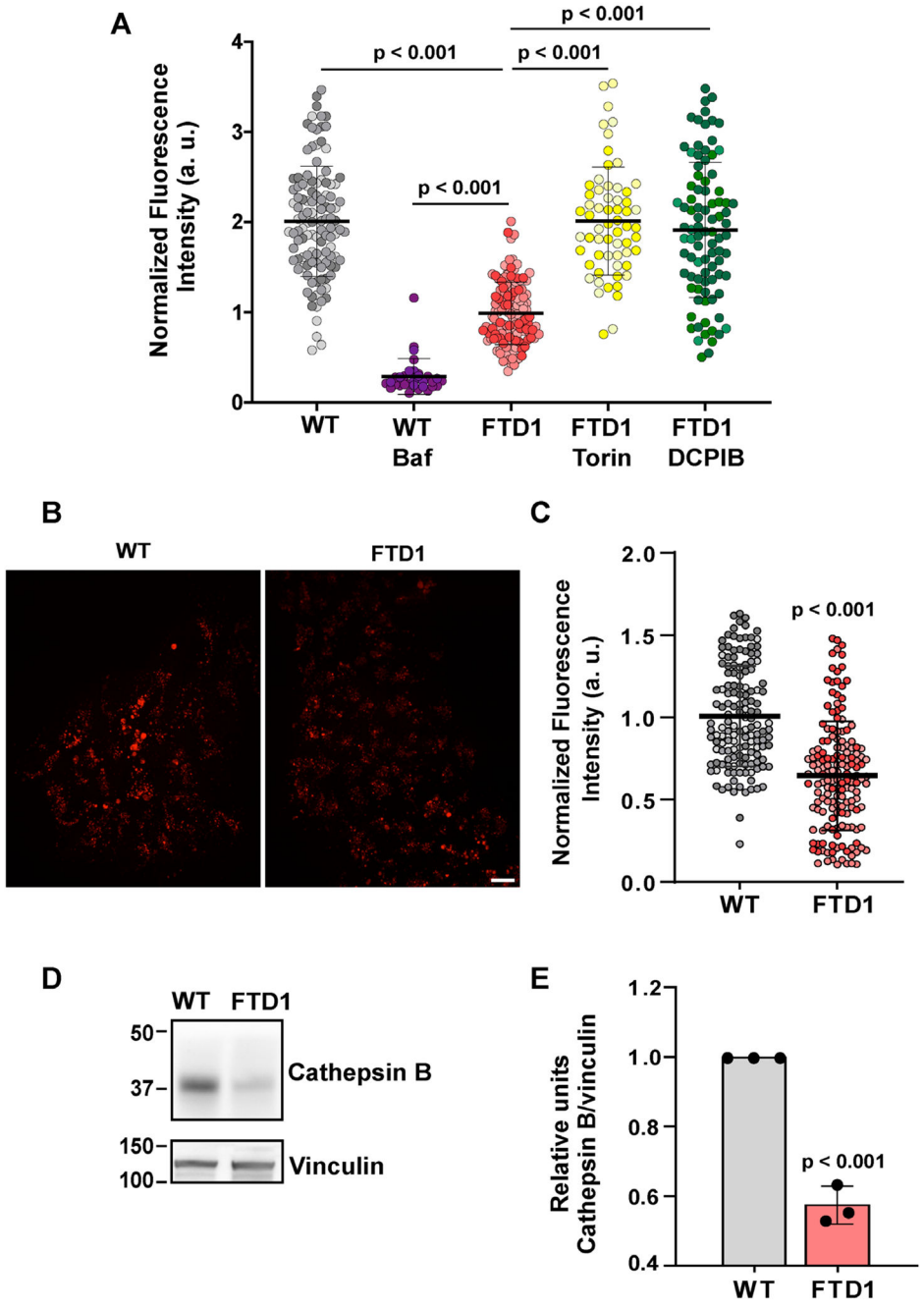

FIGURE 2:

Hydrolases and Cathepsin B activity and expression. (A) DQ-Red BSA assay of iPSCs upon treatment with different chemical drugs that modify the pHlys from three cell preparations. Different shades of the same color denote measurements from individual cell preparations. (B) Representative fluorescence microscopy images of cells stained with Magic Red, an indicator of Cathepsin B activity. Scale bar 30 μm. (C) Quantified fluorescence intensity (a.u.) of Magic Red staining. Each dot represents the fluorescence intensity measured in a randomly selected ROI, which may cover one or more cells, with data obtained from

three cell preparations. (D) Immunoblot of total cell lysates probed with antibodies for Cathepsin B, and for vinculin as a loading control. (E) Quantification of Cathepsin B immunoblotting (mean ± SD) determined from three separate cell preparations. Data are presented as normalized values, and error bars denote SD from n 3 biological replicates, relative to FTD1 control. Statistical significance was analyzed using one-way ANOVA, and p values were shown in the figure.

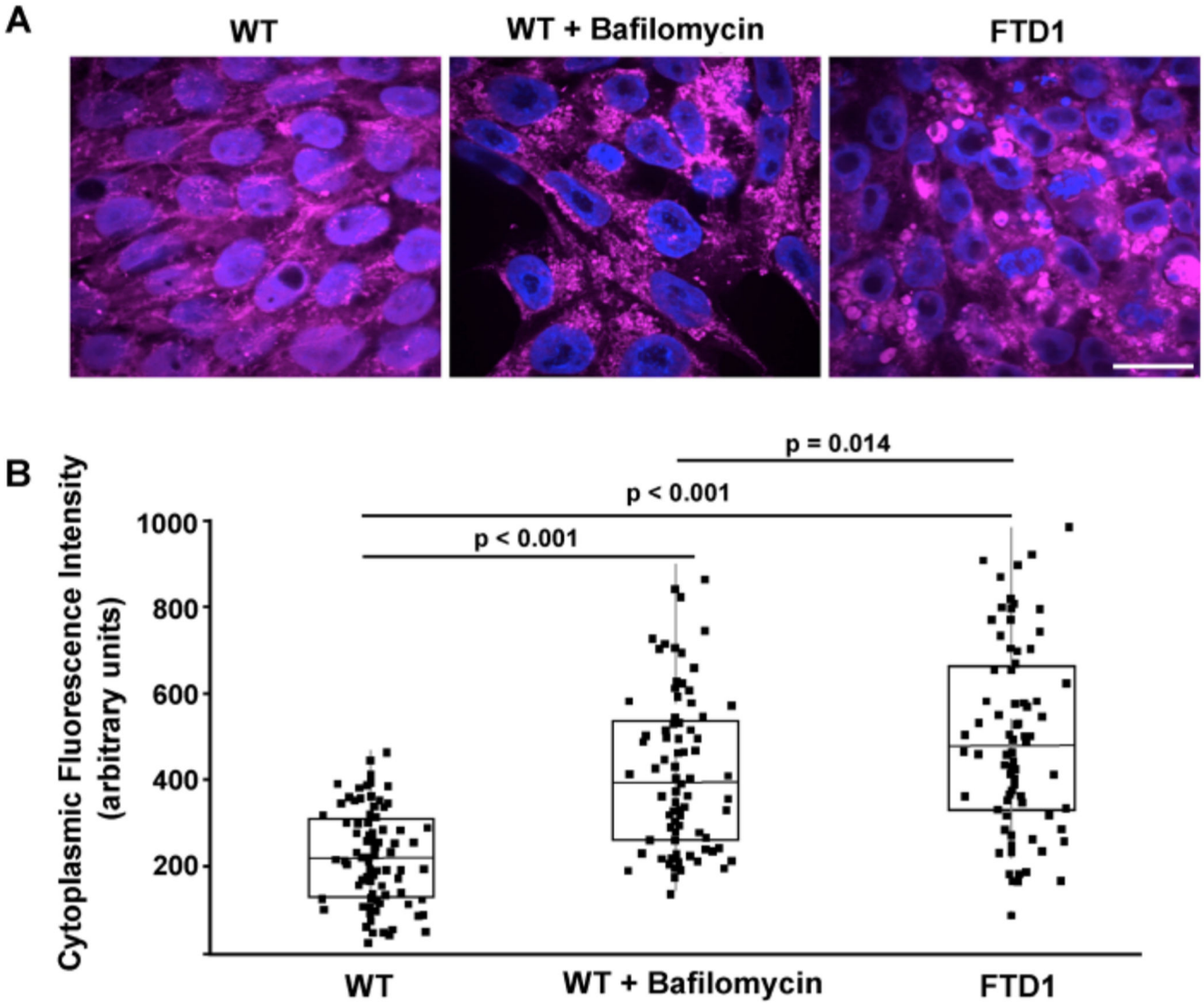

FIGURE 3:

ProteoStat labeling and aggregate quantification. (A) Representative confocal images of WT iPSCs, untreated and treated with Bafilomycin A1, and FTD1 iPSCs stained with ProteoStat (purple) and Hoechst 33342 (blue). Scale bar 10 μm. (B) Quantification of fluorescence intensities of cytosolic ProteoStat determined from images as shown in (A). Box plots show median, first, and third quartile, with whiskers extending to observations within 1.5 times the interquartile range, with data points indicating individual cells obtained from three separate cell preparations. Statistical analysis by Tukey–Kramer HSD.

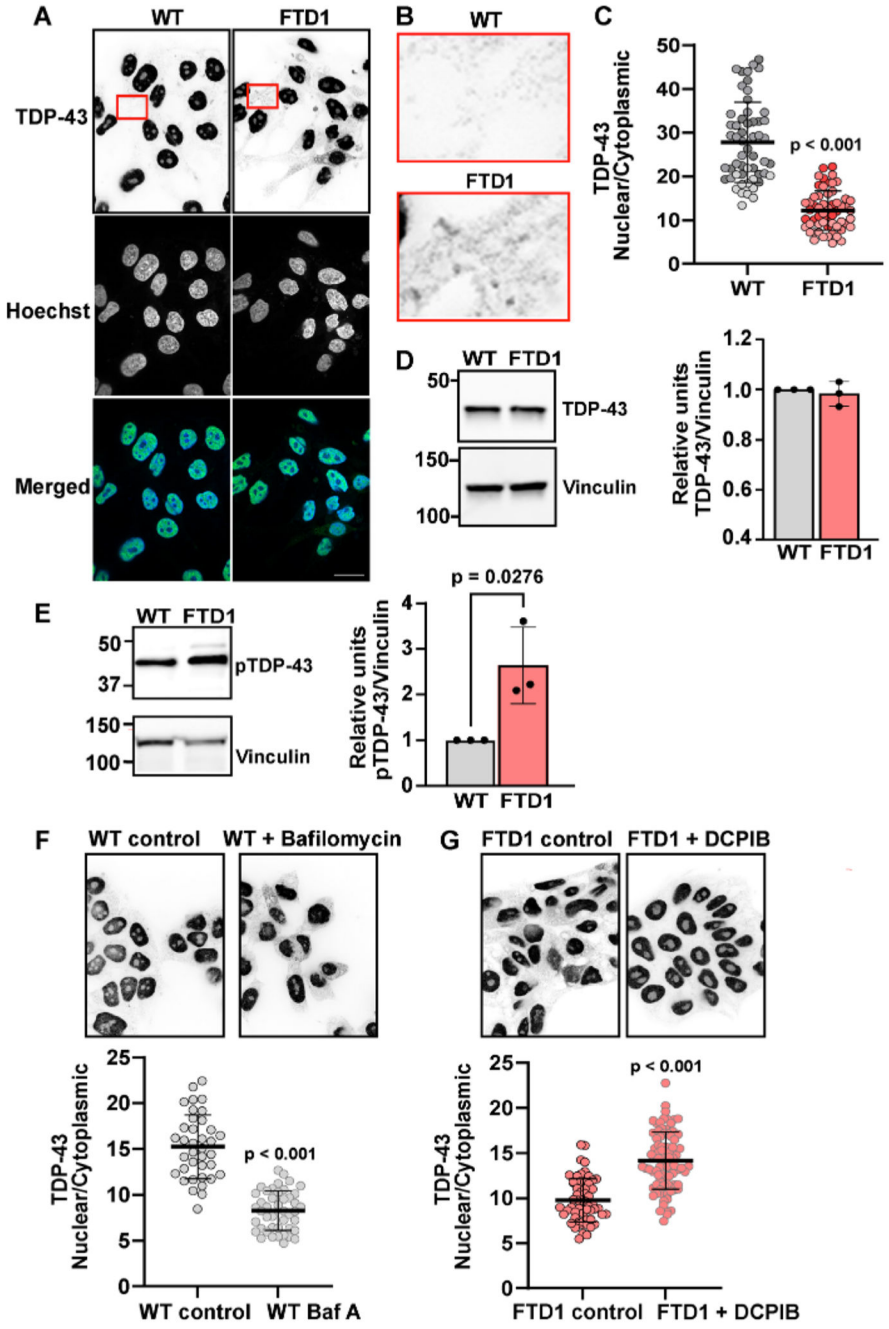

FIGURE 4:

TDP-43 localization and expression. (A) Inverted confocal images of WT and FTD1 iPSCs immunolabeled with TDP-43 and stained with Hoechst 33342. Scale bar 10 μm. (B) Higher magnification of the red-highlighted areas in (A) of TDP-43 immunolabeling. (C) Quantification of the nuclear/cytoplasmic ratio of TDP-43 fluorescence in WT and FTD1 iPSCs determined from images, as shown in (A), with each dot representing the value from a single cell. Data are from three independent cell preparations and are presented as box plots with whiskers representing minimum to maximum values. Different shades of the same

color denote measurements from individual cell preparations. Statistical significance was determined using an unpaired *t* test (p 0.001). (D) Representative immunoblots of TDP-43 with vinculin as a loading control and quantification of TDP-43 expression normalized to vinculin for immunoblots from three separate cell preparations. (E) Representative immunoblot of phosphorylated TDP-43 (pTDP-43) with vinculin as a loading control and quantification of pTDP-43 expression normalized to vinculin for immunoblots from three separate cell preparations (F and G) Inverted confocal images of TDP-43 immunolabeling and quantification of nuclear/cytoplasmic ratio of TDP-43 in WT iPSCs untreated (control) and treated with Bafilomycin (100 nM, 18 h) (F) and FTD1 iPSCs untreated (control) and treated with DCPIB (10 μM, 18 h) (G) obtained from three separate cell preparations.

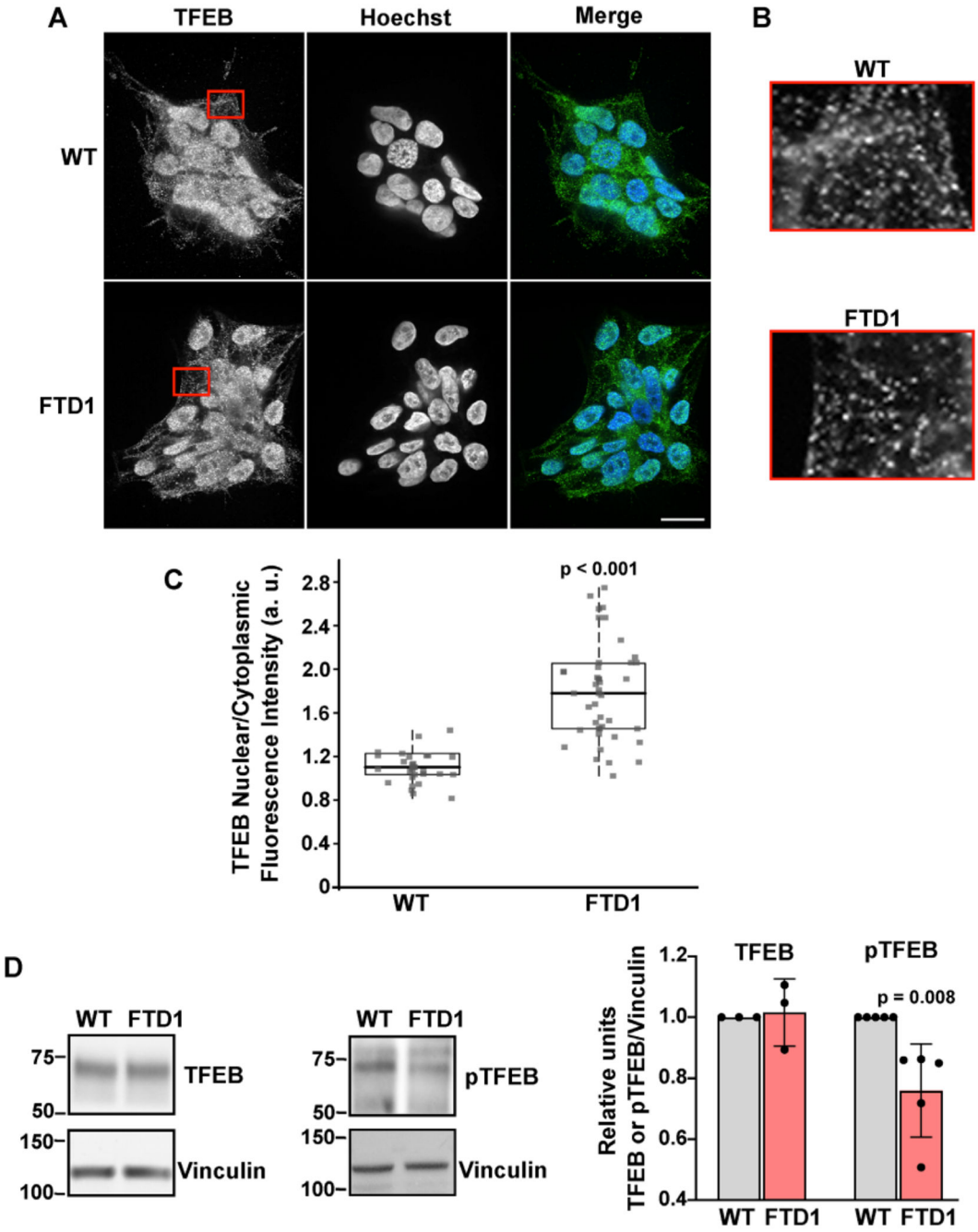

FIGURE 5:

Transcription factor EB (TFEB) localization and expression. (A) Confocal images of TFEB immunolabeling in WT and FTD1 iPSCs, stained with Hoechst 33342. Scale bar 10 μm. (B) Higher magnification of the red-highlighted areas in (A) of TFEB immunolabeling. (C) TFEB nuclear/cytoplasmic ratios in WT and FTD1 iPSCs quantified from three separate cell preparations. Each dot represents the value of a single cell. (D) Representative s and quantified data from three separate cell preparations for total TFEB and phosphorylated TFEB (pTFEB) with immunoblotting for vinculin as a loading control.

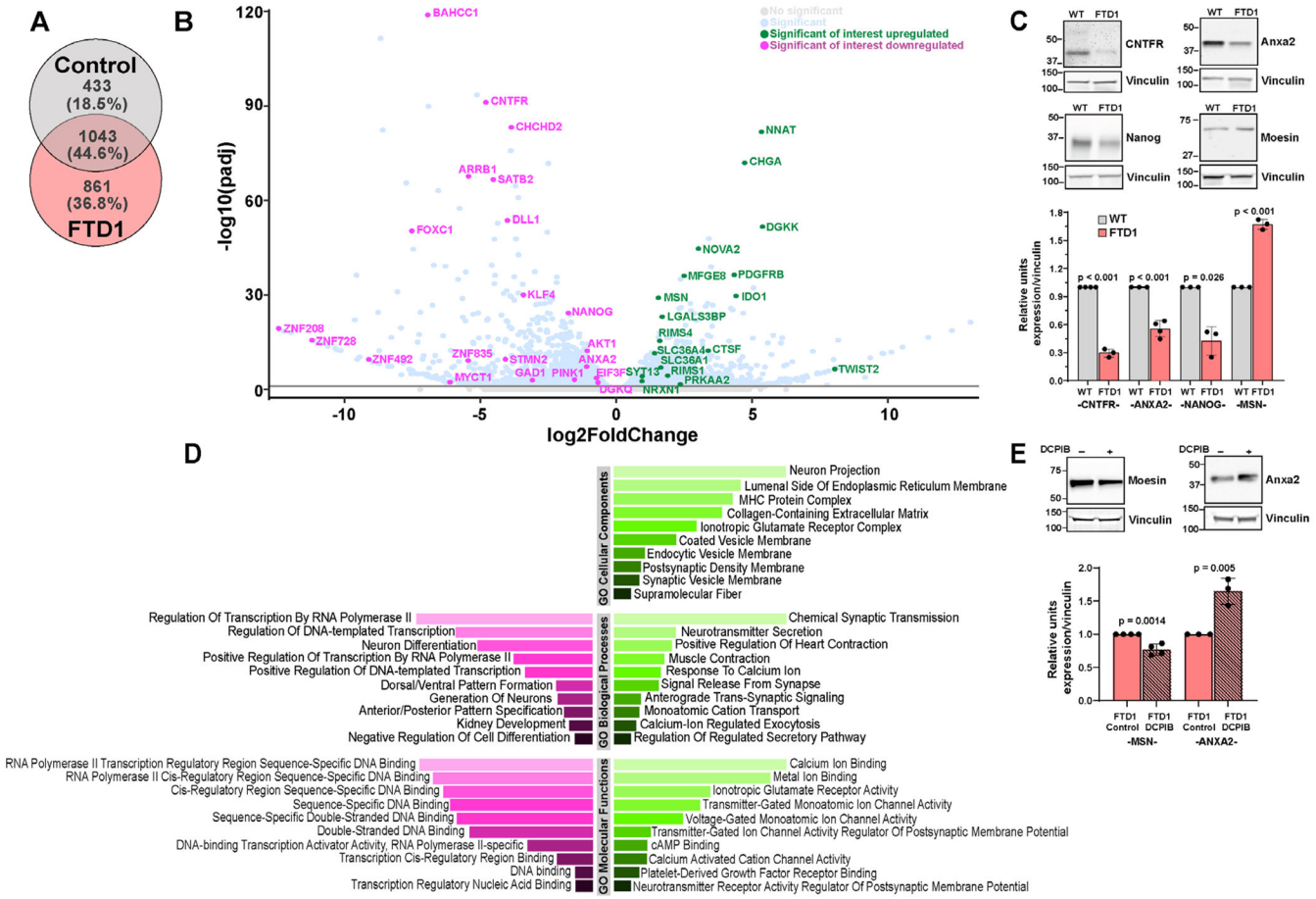

FIGURE 6:

Transcriptomic differences in WT and FTD1 iPSCs. (A) Venn diagram showing the number of shared and distinct differentially expressed genes (DEGs) in WT and FTD1 iPSCs. (B) Volcano plot showing the transcriptome fold-changes (beta values) in FTD1 compared with WT iPSCs. Each dot represents one gene, significantly changed genes (q-value 0.05) are indicated in blue. Among the significantly changed genes, those upregulated and of interest were highlighted in green while those downregulated and of interest were highlighted in magenta. (C) Immunoblots (above) and quantification (below) for the indicated proteins with vinculin used as a loading control. Quantification is presented as mean ± SEM of data from at least three separate cell preparations, with statistical significance determined by Student's *t* test. (D) Gene ontology molecular function, cellular component, and biological process enrichment analysis of upregulated DEGs uniquely indicated in FTD1 compared with WT iPSCs. RNA-seq data were obtained from three separate preparations of FTD1 and WT iPSCs. (E) Immunoblots and quantification for the indicated proteins for FTD1 and FTD1 with DCPIB, with vinculin used as a loading control. Quantification is presented as mean ± SEM of data from at least three separate cell preparations, with statistical significance determined by Student's *t* test.

TABLE 1:

Antibodies used.

Antibodies	Source	Catalogue #
Actin C4	Millipore	ZMS10004
Annexin A2	Abcam	ab41803
Cathepsin B	Abcam	EPR4323
CNTFR	ProteinTech	10796-1-AP
E-cadherin (HECD-1)	Takara	M106
Lamp1	Cell Signaling Technology	9091S
Moesin	Cell Signaling Technology	3105
NANOG	Abcam	EPR2027(2)
OCT4	Santa Cruz Biotechnology	SC-5279
Rab7	Cell Signaling Technology	9367T
SOX2	Cell Signaling Technology	3579T
TDP-43	ProteinTech	80002-1-RR
pTDP-43 (Ser409/410)	ProteinTech	22309-1-AP
TFE3	ProteinTech	14480-1-AP
TFEB	Invitrogen	PA1-31552
pTFEB	Cell Signaling Technology	37681S
TMEM175	ProteinTech	19925-1-AP
ULK1	Cell Signaling Technology	8054S
pULK1	Cell Signaling Technology	14202S
Vinculin	Millipore	V9131